Error-free and efficient prime editing in absence of maternal Polθ

François Kroll[1*], Malo Serafini[1], Luna de Barbarin[1], José Roberto Alvarez Vargas[2], Julie Thanh-Mai Dang[1], Marion Rosello[1], Marie As[2], Anne De Cian[2], Jean-Paul Concordet[2], Carine Giovannangeli[2], Filippo Del Bene[1*]

[1]Sorbonne Université, INSERM U968, CNRS UMR 7210, Institut de la Vision, Paris, France.
[2]Muséum National d'Histoire Naturelle, Sorbonne Université, INSERM U1154, CNRS UMR7196, Paris, France.

*Corresponding authors
email:
filippo.del-bene@inserm.fr
francois.kroll@inserm.fr

Abstract

Prime editing was developed to make small edits while minimising the unwanted mutations associated with genome editing based on double-strand breaks. In zebrafish embryos, however, prime editing is notably error-prone, typically yielding more unwanted mutations than precise edits. We show that virtually every unwanted mutation is generated by DNA polymerase θ (Polθ)-dependent microhomology-mediated end-joining. Loss of maternally-deposited Polθ abolishes unwanted mutations and can increase edit rates above 50%, resulting in error-free and efficient prime editing.

Owing to their rapid external development, zebrafish larvae have become widely used to model genetic diseases in biomedical research. To introduce pathogenic variants in the zebrafish genome, researchers have extensively employed homology-directed repair (HDR) of a Cas9-mediated double-strand break (DSB). Although the approach has been under development for a decade [1,2], it still achieves <10% edit rate in most cases [3,4]. Because zebrafish embryos repair most DSBs using Polθ-dependent microhomology-mediated end-joining (MMEJ), rather than HDR or non-homologous end-joining (NHEJ) [5,6], the majority of induced mutations are unwanted insertions and deletions (indels), most of which (~66%) cause frameshifts leading to premature stop codons.

Prime editing has been developed as a potentially universal approach for introducing small edits without generating DSBs [7]. It fuses a Cas9 nickase to a reverse transcriptase (RT). The guide RNA (gRNA), now called prime-editing guide RNA (pegRNA), is extended to include the primer binding site (PBS) and the template for the RT (RTT) encoding the desired edit. Cas9 nicks the genome at the locus specified by the pegRNA's spacer, releasing a 3′ end that anneals to the PBS, allowing the RT to polymerise the 3′ end using the RTT as template, thereby writing the desired edit into the genome. Previous work has shown the potential of prime editing in zebrafish [3,4,8–10]. However, reported edit rates are typically low, particularly so for substitutions (<5% per embryo), which is the largest class of human variants (>90%, Supplementary Fig. 1). In contrast to human cells, rates of unwanted indels are surprisingly high in zebrafish embryos, often several times the rate of the desired edit, undermining the main promise of genome editing without DSBs.

Here, we report that virtually every indel induced by prime editing in zebrafish was dependent on Polθ (Polq) activity during MMEJ. Prime editing in *polq* mutants can achieve edit rates above 50% and is almost perfectly precise; that is, the only observed mutation is the desired edit.

We first aimed to improve prime editing rates in zebrafish. We previously generated an albino *slc45a2* knockout line by mutating a tryptophan codon (TGG, W121) into a stop (TAA, *) [11,12]. Inspired by work on HDR [1], we reasoned that using prime editing to restore the wild-type allele (Fig. 1a) would make pigmentation reappear, providing a rapid phenotypic readout of precise (pure) edits, as most unwanted indels would not restore Slc45a2's function. To validate this "pigmentation recovery assay", we injected PE2 protein complexed with a synthetic pegRNA encoding the AA>GG edit in homozygous *slc45a2*^{W121*} embryos. At 3 days post-fertilisation (dpf), we scored eye pigmentation (Fig. 1b) and sequenced individual larvae (Supplementary Fig. 2a). We classified reads as reference, pure edit, impure edit, or scaffold incorporation if we detected pegRNA scaffold-templated nucleotides (Supplementary Fig. 2b,c). As intended, increasing pigmentation scores correlated with higher pure edit rates (1.4–8.8%, Fig. 1c) but not indels (Fig.

1d). Scores were consistent between experimenters (Supplementary Fig. 2d). The pigmentation recovery assay can therefore be used to quickly estimate precise prime editing rates.

Using this assay, we tested various injection conditions (Fig. 1e and Supplementary Fig. 3), PE protein variants (PE2, PEmax, PEmax^{L435K}, PEmax SpRY; Fig. 1f and Supplementary Fig. 4), and pegRNA modifications. Maximal edit rates (12 ± 4%; Supplementary Fig. 4c) were obtained by yolk injections of ~30 fmol of PEmax^{L435K}/pegRNA ribonucleoprotein (RNP) preassembled at a one-to-one ratio followed by incubation of the injected embryos at 28.5˚C. Neither a longer pegRNA scaffold [13,14] or a chemically modified 3′-polyuridine tail [15] substantially modified the frequency of pigmented larvae (Supplementary Fig. 5a,b), suggesting that pegRNA 3′-end degradation is not a concern in zebrafish [16].

Insertion of a riboabasic spacer between the pegRNA RTT and scaffold prevented scaffold incorporations in a nuclease-based prime-editing strategy but has not been tested with standard prime editing in zebrafish [9,17]. With the original *slc45a2* AA>GG pegRNA, 21 ± 17% of modified reads (any read that is not reference) carried scaffold-templated nucleotides (Supplementary Fig. 5c). The riboabasic spacer completely eliminated scaffold incorporations (0 ± 0%) without substantially affecting editing efficiency (70% highly pigmented larvae, vs. 82% for the original pegRNA, Supplementary Fig. 5d).

For a given edit and spacer, varying PBS and RTT lengths gives hundreds of possible pegRNAs. To optimise PBS length, it was suggested that the PBS:genome duplex Tm should approach 37˚C [10]. Reducing our *slc45a2* pegRNA PBS from 13 to 7 nt lowered its predicted Tm from 64˚C to 37˚C but decreased the rate of highly pigmented larvae from 33 to 7%, suggesting the Tm rule does not universally predict optimal PBS length (Supplementary Fig. 6a,b). As rational design is difficult, machine learning tools have been trained on human cells to predict optimal pegRNA designs. To assess these tools in zebrafish, we compiled published edit rates from 39 pegRNAs encoding 31 edits across 19 loci [3,4] and tested 12 models from DeepPrime and PRIDICT [14,18,19]. None produced a significant positive correlation between *in-vivo* edit rates and pegRNA scores, indicating that these tools do not translate to zebrafish embryos (Supplementary Fig. 6c).

Prime editing relies on generating single-strand breaks and only generates low levels of unwanted indels in human cells [3,7]. In zebrafish, however, prime editing generates surprisingly high indel rates [3]. For example, PE2 generated 1.7-fold more unwanted indels than pure edits at *slc45a2* (Fig. 1g). 81% of these indels were deletions, the other 19% were insertions (Fig. 1h). To test whether the high indel rate was specific to *slc45a2*, we tested a G>A substitution (S33L) in *ctnnb1*: PEmax generated 37 ± 18% indels, 5.7-fold more than pure edits (6 ± 5%; Supplementary Fig. 7a). The majority of these indels were again deletions (Supplementary Fig. 7c). At both loci,

indels were most frequent at the nick position, 3 bp upstream of the PAM. Indels were also frequent at the end of the RTT-templated nucleotides, which becomes a secondary nick position after RT synthesis and annealing of the 3′ flap generated by reverse transcription (Fig. 1i and Supplementary Fig. 7b).

After prime editing at *slc45a2* in wild-type embryos (GG>AA, Supplementary Fig. 8a), we noticed that the majority of unwanted deletions were flanked by microhomologies (65 ± 20% vs. 43% of simulated deletions, Fig. 1j), consistent with repair of DSBs by MMEJ. Indeed, 75 ± 25% of deletions after SpCas9 DSBs at the same locus (same spacer sequence) were also flanked by microhomologies (Fig. 1j and Supplementary Fig. 8b), in line with zebrafish embryos relying heavily on MMEJ for DSB repair [5,6]. Polθ—the key polymerase used in MMEJ—can also create insertions haphazardly templated from sequences around the break [20–22]. Half of the unwanted insertions generated during prime editing were templated from neighbouring sequences (56 ± 37% of insertion reads had a continuous match ≥6 bp between the inserted sequence and the neighbouring sequences vs. 22% of simulated insertions; Fig. 1k). This was again similar to insertions generated during repair of SpCas9 DSBs at the same locus (67 ± 42% of insertion were templated). We repeated this analysis with our pegRNA targeting *ctnnb1*: 81 ± 11% of unwanted deletions were flanked by microhomologies compared to 39% of simulated deletions (Supplementary Fig. 7d) and 50 ± 20% of insertions were templated compared to 22% of simulated insertions (Supplementary Fig. 7e). In summary, the majority of unwanted indels caused by prime editing in zebrafish show signatures of MMEJ: ~75% of deletions are flanked by microhomologies and ~50% of insertions are templated from neighbouring sequences. As MMEJ repairs DSBs by annealing microhomologies on opposite genomic strands (Supplementary Fig. 9a,b), we conclude that prime editing, even though it uses a Cas9 nickase, likely causes DSBs in the zebrafish genome.

We then explored the potential source of these DSBs. The H840A nickase—used in prime editing—reportedly retains a residual nuclease activity [23]. We first hypothesised that this was the source of the DSBs, which are then repaired by MMEJ in zebrafish embryos. As indels were frequent, H840A nickase's nuclease activity should be substantial, and therefore easily detectable. To test this *in vitro*, we incubated for 1 hr SpCas9, H840A nickase, or PEmax, with a double-stranded DNA substrate where each strand is fluorescently labelled to allow independent detection by denaturing PAGE (Fig. 2a). As expected, the non-target strand (strand opposite the gRNA) was cleaved by all three proteins. In contrast, only SpCas9 cleaved the target strand; cleavage by H840A nickase or PEmax was undetectable. We conclude that any residual nuclease activity of PEmax is not sufficient to explain the high indel rates we observed during prime editing.

The D10A nickase, which cleaves the target strand, reportedly generates much fewer DSBs than H840A nickase [23]. If most prime-editing indels were indeed caused by residual PEmax nuclease activity, the D10A nickase should therefore not cause MMEJ indels in zebrafish embryos. To test this, we targeted the pigmentation gene *tyr* using SpCas9, PE2, PEmax, H840A nickase, or D10A nickase (Supplementary Fig. 10a) [24]. SpCas9-injected embryos were all unpigmented and 99 ± 1% of reads carried an indel (Fig. 2b). The three H840A nickases —PE2, PEmax, and H840A nickase—reduced pigmentation by 42–85% and led to mutations in about half of genome copies (56–60% indel rate). The D10A nickase was in fact more mutagenic than the H840A nickases, reducing pigmentation by 94% and pushing indel rate to 79 ± 10% (Fig. 2b and Supplementary Fig. 10b). This is in stark contrast to D10A nickase activity in mammalian cells where it rarely causes indels [20,25]. Every protein caused a majority of microhomology-flanked deletions (Fig. 2c), from 66% of deletion reads for PE2 to 83% for D10A nickase. To test whether these observations also applied to base editing, which relies on target-strand cleavage by D10A nickase, we reanalysed a published experiment that tested the base editor AncBE4max [11,26]. AncBE4max mRNA generated 22 ± 5% unwanted indels (Supplementary Fig. 11a). In line with our results, 75 ± 4% of the deletions were flanked by microhomologies (Supplementary Fig. 11b).

As target-strand cleavage by PEmax was undetectable *in vitro* and that D10A nickase also caused microhomology-flanked deletions in zebrafish embryos, we conclude that most MMEJ-repaired DSBs were not directly made by PEmax. Moreover, H840A nickase without RT and PEmax/gRNA both generated MMEJ indels, excluding an indel-causing mechanism involving the RT or the prime-editing flaps [27]. Instead, we propose that nicks are converted into DSBs endogenously by replication forks. When a replication fork arrives at a nick, daughter strand synthesis is interrupted because the template strand is broken, leading to a DSB [28–32]. During the first three hours after fertilisation, zebrafish embryos divide extremely quickly (every ~15 min) [33–36], creating a high chance of collision between nicks and replication forks. In human cell cultures, prime editing generates much fewer indels [3,7], possibly because cell cycle is ~100× slower (24 hr vs. 15 min). Across species and cell types, the probability to generate a DSB during nick-based genome editing may depend partly on cell cycle length.

As most prime-editing indels seemed created by MMEJ, we wondered whether inhibition of MMEJ would reduce indels. Polθ—encoded in zebrafish by *polq*—is essential to MMEJ but homozygous knockout (KO) zebrafish are fertile [5,6]. As mRNA of *polq* and other MMEJ factors are maternally deposited (Supplementary Fig. 12) [5], we used maternal mutant embryos to prevent MMEJ early in development. We tested a one-bp substitution (G>C in *cacng2b*) in wild-type embryos, maternal-only heterozygous mutants (offspring of an outcross homozygous *polq* KO mother × wild-type father), and maternal-zygotic homozygous *polq* mutants (offspring of a homozygous *polq* KO incross) (Fig. 2d). In wild-type embryos, pure edit rate was 13 ± 6% but indel rate was 1.6-fold higher (21 ± 11%). Strikingly, indels were completely absent in maternal-

zygotic *polq* mutants (0 ± 0%) and rare in maternal-only mutants (0.7 ± 1.2%). The pure edit rate also surged in *polq* mutants, reaching 45 ± 25% in maternal-only mutants and 53 ± 28% in maternal-zygotic mutants.

We tested a total of 9 edits across three loci (Supplementary Fig. 13): *cacng2b*, *adgrf3b*, and *slc45a2*. Total absence of Polθ abolished nearly all indels (Fig. 2e; maximum 1.6 ± 1.0% for *slc45a2* GG>AA in maternal-zygotic KO). The dependence on Polθ to generate deletions was close to absolute: we only found 11 deletion alleles in 31,568 sequencing reads; 8 of which had no or 1-bp microhomologies, which may be expected by chance (Supplementary Fig. 14). There were just 8 insertion alleles left, all 1–6 bp, demonstrating that all templated insertions were dependent on Polθ, not on the RT as previously hypothesised [3]. Maternal-only mutants had similarly low indel rates (maximum 4 ± 3% for *adgrf3b* C>G, all others <1%, see Supplementary Note 1). Interestingly, absence of Polθ also eliminated scaffold incorporations at *slc45a2* (4 ± 5% in wild types, 0 ± 0% in n = 21 *polq* mutants, see Supplementary Note 2). Effects on edit rates were often drastic too (Fig. 2e): for 3/9 edits, pure edit rates raised >50% in maternal-zygotic KO, with almost half of samples (11/28) even reaching >70% pure edits. Pure edit rates were largely unchanged for 4/9 edits (<15% difference) but declined for 2/9 (−18, −26%). Maternal-only mutants gave similar edit rates as maternal-zygotic ones (6/7 edits with <15% difference with maternal-zygotic KO). Using heterozygous (maternal-only) *polq* mutants thus provides most benefits from MMEJ inhibition while allowing edited animals in wild-type background to be created in the F1.

Without Polθ, are DSBs repaired by a mechanism that is far less mutagenic than MMEJ (e.g., NHEJ or HDR) or are DSBs simply left unrepaired? If the latter is true, cells harbouring a DSB should eventually enter apoptosis. We used acridine orange to stain apoptotic cells in wild-type, maternal-zygotic, and maternal-only *polq* mutant embryos injected with a non-targeting pegRNA or with the *slc45a2* GG>AA pegRNA (Fig. 2f). Prime editing in wild-type embryos, independently of injections, caused some apoptosis as the number of acridine-positive puncta increased slightly (1.4-fold) compared to the non-targeting pegRNA-injected embryos. This effect was stronger in absence of maternal Polθ, with apoptotic cells rising 2-fold in maternal-only mutants and 2.8-fold in maternal-zygotic mutants. To compare these to other forms of DNA damage, we exposed wild-type embryos to cadmium, a mutagenic heavy metal; AOH1160, a PCNA inhibitor; or UV radiation. The number of acridine-positive puncta increased from 4 to 12-fold (Supplementary Fig. 16). We propose that prime-editing nicks are converted to DSBs which are left unrepaired when maternal Polθ is not available, pushing cells harbouring a DSB to enter apoptosis, eventually leaving only wild-type and correctly edited cells.

Finally, to confirm germline transmission of the prime edits in *polq* mutants, we injected maternal-only mutants with a PEmax^{L435K}/*slc45a2* GG>AA RNP, grew larvae with patches of

depigmentation, and sequenced their offspring (Fig. 2g). All six animals tested transmitted the GG>AA edit at rates 1.5–78%, confirming that prime editing in *polq* mutants can be used to establish stable lines.

The promise of nick-based genome editing like prime editing is to limit unwanted indels by avoiding DSBs. However, prime editing in zebrafish embryos is highly error-prone, in some cases generating as many indels as genome editing based on Cas9 nuclease. We show that almost every prime-editing indel was created by Polθ-dependent MMEJ. Consequently, prime editing in *polq* knockouts achieves virtually perfect precision and can lead to edit rates >50%, considerably expanding the use of zebrafish as model for genetic diseases and functional genomics. In the future, error-free prime editing may prove useful for lineage tracing [37] and F0 phenotyping if edit rates can be raised further [38]. Our finding that D10A nickase also causes high rates of indels with signature of MMEJ suggests that precision of other nick-based genome editing methods, such as base editing and nickase-based HDR [39], could also benefit from Polθ inactivation. This may also be true for many model organisms, such as Drosophila, Xenopus, and *C. elegans*, whose embryos also have rapid cell cycles (respectively 9, 30, 15–50 min) [40–42] and can repair DSBs by MMEJ [43–45].

Supplementary Note 1

Absence of maternally-deposited *polq* mRNA/Polθ protein drastically reduced indel rates, even when the embryo inherited a functional *polq* gene from its father (Fig. 2e). This wild-type paternal copy becomes active after the maternal-to-zygotic transition around 5 hpf (Supplementary Fig. 13), but seemingly does not create many indels. This observation leaves two possible options: either every break is repaired within the first 5 hours and PEmax does not make new breaks after that; or repair of nicks/DSBs does not leave indels after 5 hpf. The first option is unlikely as ample wild-type genome copies remain and the PEmax RNP is probably still present at sufficient concentrations in cells to make breaks for many hours or even days after injection. For example, to test a photoactivable CRISPR system, Hu et al. (2025) injected one-cell stage embryos with 6 fmol of inactivated Cas9/gRNA RNP then exposed the 2-dpf larvae (48 hours after injection) with UV to activate the RNPs, which still caused indels in ~35% of genome copies [46]. In our case, assuming no degradation of the RNPs, if 18 billion RNPs (30 fmol) injected at the one-cell stage are distributed equally during 13 divisions (5 hpf), each cell at this 8k-cell-stage would contain 2.2 million RNPs. In comparison, a very abundant transcription factor is found at 300,000 molecules per cell [47]. After the 10th cell division, which coincides with the start of the maternal-to-zygotic transition [36], cell cycle length slows down [33,34]. This may explain why, after 5 hpf, new breaks by PEmax are repaired without leaving indels: replication forks are now less frequent, so the probability of collisions with nicks is low, leaving enough time for nicks to be repaired before they are converted into DSBs. Accordingly, we predict that applications using prime editing later in development, for example for tissue-specific genome editing, would generate lower indel frequencies, as is observed in human cells.

Supplementary Note 2

Absence of Polθ eliminated scaffold incorporations at the *slc45a2* locus (4 ± 5% in wild-type larvae, 0 ± 0% in n = 21 *polq* mutants, Supplementary Fig. 13), but paradoxically our results indicate that the RT frequently proceeds past the end of the RTT without the riboabasic spacer, at least at the *slc45a2* locus (Supplementary Fig. 5c). It may be that the RT regularly writes a scaffold-templated sequence in the edited 3′ flap, which is then installed in the genome as an insertion by Polθ taking the flap as template. In absence of Polθ, the edited 3′ flap may correctly anneal to the genome, pushing its scaffold-templated end as a flap that is then excised like the unedited 5′ flap. Some scaffold incorporations indeed looked like MMEJ insertions (Supplementary Fig. 15), consisting of a patchwork of scaffold-templated sequences sometimes followed by sequences that exist earlier in the RTT. At the *slc45a2* locus, the end of the RTT-templated nucleotides matches the start of the scaffold (edited 3′ flap should end with GGAGA, first scaffold-templated nucleotides are expected to be GGA), which may facilitate the annealing of microhomologies. It remains to be seen whether absence of Polθ also eliminates scaffold incorporations at other loci.

Methods

Animals

Adult zebrafish (*Danio rerio*) were reared in Institut de la Vision (Paris, France) fish facility at 25°C on a 14 hr:10 hr light:dark cycle with gradual lights-on and lights-off transitions to simulate sunrise and sunset. To obtain eggs, male and female zebrafish were isolated in breeding boxes overnight, separated by a divider. Around 10 AM the next day, the dividers were removed and eggs were collected. The embryos were then raised in 10-cm Petri dishes filled with egg medium (0.3 g/L Instant Ocean and 0.00005% methylene blue) in a 28.5°C incubator on a 14 hr:10 hr light:dark cycle. Debris and dead or dysmorphic embryos were removed every other day with a Pasteur pipette under a bright-field microscope and the fish water replaced. At the end of the experiments, larvae were euthanised with an overdose of tricaine (MS-222, Sigma-Aldrich).

All animal procedures were performed in accordance with French and European Union animal welfare guidelines and were approved by the Animal Experimentation Ethics Committee of Sorbonne Université (APAFIS#21323- 2019062416186982 and APAFIS #49266-2024050214115020) (number 005).

Wild types refer to TL (Tüpfel long fin) zebrafish. The *polq* KO line was generated by Carrara et al., 2025 [5]. Using Sanger sequencing, we independently verified the mutation to be a 219-bp deletion spanning exon 6 and exon 7/32 (chr21:22,866,462–22,866,680 on reference genome GRCz11). We genotyped animals by running *polq* amplicons on a 1% agarose gel stained with ethidium bromide (Dutscher). PCR primer sequences were from Carrara et al., 2025 and are provided in Supplementary File 1. Maternal-zygotic homozygous *polq* KO refers to offspring of an incross where both parents were homozygous *polq* KO. Maternal-only heterozygous *polq* KO refers to offspring of an outcross where the mother was homozygous *polq* KO and the father was TL wild-type.

Synthesis of PE proteins

We adapted a protocol for synthesis of SpCas9 [48]. The protocols will be described in a subsequent publication (Alvarez Vargas et al., 2026. *in preparation*). Except for PE2, all PE proteins used in this work were based on the PEmax architecture [49]. pET28-PE-His6 plasmid was introduced in Rosetta 2(DE3) competent cells (Sigma-Aldrich) for protein expression. A three-step purification was performed using HisTrap affinity chromatography followed by cation and anion exchange columns. PE protein stocks were prepared in 20 mM HEPES pH 7.5, 350 mM KCl, 1 mM TCEP, 10% glycerol at 60 µM for PE2, 60–90 µM for PEmax, 70 µM for PEmax SpRY, 90 µM for $PEmax^{L435K}$. Stocks were stored at −80˚C or −20˚C before use.

Preparation and injection of PE/pegRNA RNP

Synthetic pegRNAs were bought from Integrated DNA Technologies (IDT) as “Custom CRISPR gRNA” with standard desalting purification and without Alt-R modifications. Sequences are provided in Supplementary File 1. Each pegRNA was received as a pellet which was resuspended in Duplex buffer

(IDT) to form a 100 µM stock. Aliquots of this stock were stored at −80˚C before use. On the morning of injections, the pegRNA was mixed with the PE protein in equimolar proportions (e.g., 0.6 µL Duplex buffer; 0.9 µL pegRNA 100 µM; 1.5 µL PE protein 60 µM) and the mix was incubated at 37˚C for 5 min then cooled on ice to generate a 30 µM PE/pegRNA RNP solution. Approximately 1 nL of this RNP solution (i.e., 30 fmol RNP) was injected into the yolk at the one-cell stage before cell inflation.

slc45a2 AA>GG pegRNA with riboabasic spacer ("rSpacer") used in Supplementary Fig. 5c was bought from Horizon Discovery with HPLC purification. The PEmax^{L435K}/pegRNA RNP was prepared and injected as above.

The spacer sequences of the *cacng2b* and *adgrf3b* pegRNAs were taken from Petri et al., 2025. The *cacng2b* G>C pegRNA had the same sequence as the one used by Petri et al., 2025; others were modified. The following edits inactivated the PAM: *cacng2b* G>C, *cacng2b* 6-bp deletion, *adgrf3b* C>G, *adgrf3b* 3-bp deletion. The following edits did not inactivate the PAM: *slc45a2* AA>GG, *slc45a2* GG>AA, *ctnnb1* G>A, *cacng2b* 3-bp deletion, *cacng2b* 3-bp insertion, *cacng2b* 6-bp insertion, *adgrf3b* 3-bp insertion. All *cacng2b* and *adgrf3b* pegRNAs carried a 3′ polyuridine (UUUU) tract; others did not, except for the *slc45a2* pegRNA with optimised 3′ end (Supplementary Fig. 5a). pegRNA sequences can be found in Supplementary File 1.

In the experiment testing an excess of pegRNA (Supplementary Fig. 3a), the pegRNA was resuspended in Duplex buffer to form a 200 µM stock so that the pegRNA could be added in higher amounts.

In the experiment testing RNP doses (Fig. 1e), we prepared a 20 µM RNP solution as above and diluted some to make a 2.5 µM RNP solution by adding a 1:1 mix of Duplex buffer and protein buffer (20 mM HEPES pH 7.5, 350 mM KCl, 1 mM TCEP, 10% glycerol). We then injected 0.5, 1.0, 1.5 nL of the 2.5 µM solution, which amounts to 1.25, 2.5, 3.75 fmol RNP; and 0.5, 1.0, 1.5, 2.0 nL of the 20 µM solution, which amounts to 10, 20, 30, 40 fmol RNP. In a separate experiment, we prepared a 40 µM RNP solution as above and injected 0.5, 1.0, 1.5, 2.0 nL, which amounts to 20, 40, 60, 80 fmol RNP. We also injected 3 nL (120 fmol RNP) of this solution but too few larvae (6/43) survived until 3 dpf to be analysed. For the common doses, results from both experiments replicated even though volume injected varied (less than ± 10% difference in proportion of highly pigmented larvae).

In the experiment testing different sites of injections (Supplementary Fig. 3b), eggs taken from the same batch were injected in the yolk; or in the single cell before inflation; or in the single cell after it inflated; or in both cells after the first division (1 nL in each cell).

Pigmentation recovery assay

The *slc45a2*^{W121*} mutant line was generated by base editing in our previous work [11]. *slc45a2*^{W121*} homozygous embryos were injected at the one-cell stage with PE RNP encoding the TAA(*)>TGG(W)

edit to restore the wild-type (TGG) allele. At 3 dpf, each larva was scored on a scale from 0 to 5 mainly based on its eye pigmentation: score 0 if the larva was as unpigmented as *slc45a2*^{W121*} homozygous larvae; score 1 if the eye was unpigmented but the larva had some pigmented cells elsewhere; score 2 if the eye had a single patch of pigmented cells; score 3 if more than approximately a third of the surface of the eye was pigmented; score 4 if most of the eye surface was pigmented. To avoid any bias in case one eye was pigmented but the other was not, only the right or left eye was scored during a given experiment. All scoring was done blinded to the condition. Dysmorphic larvae were scored if their eyes were sufficiently developed. Viability reports the number of larvae looking healthy at the end of the experiment (3–6 dpf) divided by the total number of injected embryos at 0 dpf; that is, including any unfertilised eggs or embryos damaged by the injection needle. Larvae that had not hatched naturally from the chorion at 3 dpf were counted as unviable. To exclude loss of viability unrelated to the experiment (e.g., unfertilised eggs), we divided this proportion to the viable proportion of uninjected embryos of the same experiment.

Targeting *slc45a2* or *tyr* with SpCas9 or Cas9 nickases

The synthetic *tyr* gRNA was made of two components which were bought separately from IDT: the crRNA (Alt-R CRISPR-Cas9 crRNA) and tracrRNA (Alt-R CRISPR-Cas9 tracrRNA). The crRNA sequence was taken from our previous work [50]. The crRNA and tracrRNA were received as pellets, which were individually resuspended in Duplex buffer (IDT, received with the tracrRNA) to form 200 µM stocks. Stocks of crRNA and tracrRNA were stored at −80 °C before use. The crRNA was annealed with the tracrRNA by mixing 3.7 µL crRNA 200 µM; 3.7 µL tracrRNA 200 µM; 4.6 µL Duplex buffer. The mix was heated to 95˚C for 5 min, then cooled on ice, to obtain a 61 µM gRNA (crRNA/tracrRNA duplex) solution. For each protein (SpCas9, PE2, PEmax, H840A nickase, D10A nickase), 2 µL of the gRNA solution were mixed with 2 µL of protein at 60 or 61 µM. SpCas9 (Alt-R S.p. Cas9 Nuclease V3), H840A nickase (Alt-R S.p. Cas9 H840A Nickase V3), and D10A nickase (Alt-R S.p. Cas9 D10A Nickase V3) were bought from IDT. PE2 and PEmax proteins were synthesised in house (see *Synthesis of PE proteins*). Each mix was incubated at 37°C for 5 min then cooled on ice, generating six 30 µM RNP solutions. Approximately 1 nL of each solution (~30 fmol RNP) was injected in the yolk at the one-cell stage. Targeting *slc45a2* with SpCas9 followed the same steps as above. The crRNA sequences are provided in Supplementary File 1.

For the experiment targeting *tyr*, we photographed the injected larvae at 2 dpf under a brightfield microscope (see *Pictures*). To speed up the process, we photographed multiple larvae in the same field of view. The images were then segmented into pictures of individual larvae using a YOLO v8 (ultralytics v8.3.7) model [51] trained on 350 images manually annotated using app.roboflow.com. We then counted, for each picture, the number of pixels with grey value ≤116 (0 is black, 255 is white) using the R package ijtiff, returning the number of dark pixels plotted in Supplementary Fig. 10b.

Germline transmission of *slc45a2* GG>AA

Maternal-only heterozygous *polq* KO embryos were injected at the one-cell stage with 30 fmol of PEmax^{L453K}/*slc45a2* GG>AA pegRNA RNP. At 3 dpf, larvae with patches of eye depigmentation visible

under a brightfield microscope were selected to be grown. Adults were then crossed to wild-type animals and we extracted genomic DNA from pools of 20–40 F1 embryos (see *Preparation of samples for deep sequencing*). From the genomic DNA, we amplified a 546-bp amplicon spanning exon 1/7 of *slc45a2* (primer sequences in Supplementary File 1). Amplicons were sent to Plasmidsaurus for Nanopore sequencing (PCR Premium Standard service). We aligned the fastq reads to the reference amplicon sequence using minimap2 v2.22. To calculate the rate of GG>AA edit, we counted the number of AA reads in IGV and divided this count by the total number of reads at this position. We also calculated edit rates using the CRISPRLungo web interface [52] and found that both methods gave a <1% difference in edit rates for every sample. As the F0 injected animals were crossed to wild types to generate the F1 offspring sequenced, the true germline transmission rate is expected to be double the edit rates measured in the F1; Fig. 2g therefore reports double the measured edit rates.

Preparation of samples for deep sequencing

Individual larvae were anaesthetised with tricaine (MS-222) and their genomic DNA extracted by HotSHOT [53] as follows. Individual larvae were transferred to a 96-well PCR plate or strips of 8 tubes. Excess liquid was removed from each well before adding 50 µL of 1× base solution (25 mM KOH, 0.2 mM EDTA in water). Plates were sealed and incubated at 95°C for 30 min then cooled to room temperature before the addition of 50 µL of 1× neutralisation solution (40 mM Tris-HCl in water). Genomic DNA was then stored at –20°C.

PCR primers were designed for each target locus using Primer-BLAST (NCBI) to amplify a window of 150–200 bp with at least 20 bp between each primer binding site and the predicted cut site. PCR primers were ordered with a Nextera overhang at the 5′ end of each primer to allow indexing (see Supplementary File 1). Some PCR primer sequences were taken from previous studies [3,50].

Each PCR well contained: 5.13 µL dH2O, 1.8 µL 5× Phusion HF buffer (New England Biolabs), 0.3 µL DMSO, 0.18 µL dNTP (10 mM), 0.45 µL forward primer (10 µM), 0.45 µL reverse primer (10 µM), 0.09 µL Phusion High-Fidelity DNA Polymerase (New England Biolabs), 1.0 µL genomic DNA; for a total of 9.4 µL. The PCR plate was sealed and placed into a thermocycler. The PCR program was: 98°C – 5 min, then 40 cycles of: 98°C – 10 sec, 60°C – 30 sec, 72°C – 30 sec, then 72°C – 10 min, then cooled to 10°C until collection. The PCR product's concentration was quantified with Qubit (dsDNA Broad Range Assay) and its length was verified on a 1% agarose gel with ethidium bromide (Dutscher). Excess primers and dNTPs were removed by ExoSAP-IT (Thermo Fisher) following the manufacturer's instructions. The samples were then sent for Illumina MiSeq, which used MiSeq Reagent Nano Kit v2 (300 Cycles).

Sequencing analysis of prime-editing samples

Illumina MiSeq data was received as two fastq files for each well, one forward and one reverse. The paired-end reads were aligned to the reference amplicon with bwa v0.7.18 and the resulting bam alignment file was sorted and indexed with samtools v1.6 [54]. Alignments were then filtered to keep only reads with less than 20% of their length soft-clipped and spanning at least 90 bp of the reference

sequence and 30 bp on each side of the predicted cut site. To check the alignment and filtering steps, bam alignment files were visualised with IGV v2.16.2. The resulting filtered bam file were converted back to forward and reverse fastq files using bedtools v2.30.0 [55]. These filtered fastq files were used as input to CRISPResso2 v2.2.15 [56] ran in command line. CRISPResso2 was ran for each pair of fastq files in standard amplicon mode—not in prime-editing mode—to produce alignments. From CRISPResso2's output, each *Alleles_frequency_table.txt* file was used as input for our custom "CUTTER" (the CRISPR mutations caller) R package available at github.com/francoiskroll/cutter. Briefly, function callMutations(…) produced a csv table listing all mutations on individual reads by calling insertions, deletions, and substitutions for each alignment. Any mutation that was found in fewer than three reads or was not within ± 12 bp of the cut (and ligation position for prime-editing samples) was excluded. The function classifyReads(…) was then ran on the mutation table to assign every read to one of the following labels: "pure" if only the expected edit was present; "impure" if the expected edit and some indel(s) were present; "indel" if the expected edit was not present (including if the edit position was deleted) and some indel(s) were present; "scaffold" if nucleotides likely templated from the pegRNA scaffold were present directly after the ligation position; or "reference" if no other label was called. The scaffold label trumped all others. For example, scaffold reads usually included the expected edit but were labelled scaffold, not pure or impure. Detection of scaffold-templated nucleotides is complex as one needs to consider both substitutions and insertions (Supplementary Fig. 2c), different scaffold sequences, and whether the reference happens to match the expected scaffold-templated nucleotides after the ligation position. Details about the detection can be found in the GitHub documentation. To avoid calling sequencing errors, substitutions that were not the expected edit or likely scaffold-templated were ignored in the classification; that is, a "reference" read may include substitutions. Figures like Fig. 1g plots, for each sample, the proportion of reads assigned to each label.

Indel positions

This refers to Fig. 1i and Supplementary Fig. 7b. Scaffold insertions were excluded from the analysis. To simplify the frequency calculations, we also excluded any read that had more than one indel, which were 311/3028 (10%) for *slc45a2* and 1836/38,553 (5%) for *ctnnb1*. To avoid extrapolating frequencies from too few reads, we excluded any sample with fewer than 50 reads with an indel, this excluded 1/10 samples for *slc45a2* and 1/49 samples for *ctnnb1*. We first computed the frequency of each indel within each sample (number of reads with this indel/total number of reads with an indel), then computed the average frequency of each unique indel across every sample (animal) from each locus, returning one frequency for each indel at each locus. If a sample did not have a given indel, we added a frequency = 0 for this indel in the average frequency calculation. For example, if indel X was only present as 5% of indel reads in one of the nine *slc45a2* samples, we would calculate the average frequency of indel X as the mean of 0.05, 0, 0, 0, 0, 0, 0, 0, 0 (= 0.0056). This calculation sets the total frequency in each plot to be 1.0. Each indel was plotted at a single position: for deletions this was the start of the deletion, which is the most 5′ deleted nucleotide; insertions are set by CUTTER as having the same start and stop position.

482 **Detection of deletions flanked by microhomologies**

483 The general mutation pattern to be detected was *right microhomology—inner sequence—left*
484 *microhomology* in the reference sequence with the deleted sequence in the aligned read being *right*
485 *microhomology—inner sequence* (i.e., *left microhomology* retained) or *inner sequence—left*
486 *microhomology* (i.e., *right microhomology* retained). 1-bp microhomologies were accepted but the
487 algorithm was designed to always return the longest possible microhomologies. The detection
488 algorithm tested both options (left or right microhomology retained). In occasional cases where both
489 options returned a possible microhomology, the algorithm returned the longest (i.e., most convincing)
490 microhomology. In rare cases where both options gave the same microhomology length, the algorithm
491 returned the right microhomology retained option. Note that right or left microhomology retained
492 may be an arbitrary decision by the alignment algorithm rather than reflect the DNA repair
493 mechanism.

494

495 A deletion may be flanked by microhomologies by chance, rather than reflecting repair by MMEJ. This
496 is especially the case as we accepted 1-bp microhomologies: in a random sequence (0.25 chance of
497 each nucleotide), 50% of deletions would technically be flanked by 1-bp microhomologies according to
498 our definition; that is, 0.25 chance that the last nucleotide before the deletion matches the last
499 nucleotide of the deleted sequence (left microhomology retained) + 0.25 chance that the first
500 nucleotide of the deleted sequence matches the first nucleotide after the deletion (right
501 microhomology retained). In practice, the expected probabilities of observing microhomologies by
502 chance will vary by locus. For example, deletions in a highly repetitive sequence will more frequently
503 be flanked by chance microhomologies. To estimate these null probabilities, we simulated 1000 reads
504 with a deletion for each locus. To simulate each deletion read, we first drew a length from a
505 distribution of deletion lengths that is typical from repair of Cas9 DSBs in zebrafish embryos
506 (Supplementary Fig. 17a; see *Fitting distributions of deletion and insertion lengths*). If the length was
507 3 bp or longer, we considered every deletion of this length that removed the nucleotide that is just 5′
508 of the expected cut position and drew one deletion at random. If the length was 1 or 2 bp, we
509 considered every deletion of this length that removed at least a nucleotide that is within 4 bp of the
510 expected cut position (i.e., at most 3 bp separating a deleted nucleotide from the nucleotide 5′ of the
511 expected cut position) and drew one deletion at random. We then detected microhomologies from
512 these 1000 simulated reads carrying a deletion as above.

513

514 **Detection of insertions templated from neighbouring sequences**

515 Polθ-mediated insertions are often a patchwork of sequences templated from neighbouring sequences
516 (e.g., Supplementary Fig. 15); therefore, naively searching for the entire newly synthesised sequence in
517 neighbouring sequences would rarely map the origin of the inserted sequence. Rather, we aimed for
518 the analysis to extract the longest continuous match between the newly synthesised sequence
519 (insertion and any accompanying substitution(s)) and its neighbouring sequences. To define the
520 neighbouring sequences, we centred the search window on the centre of the newly synthesised
521 sequence. Insertions are set by CUTTER to have the same start and stop position, but an
522 accompanying substitution could shift this centre position. The search window on the reference

523 sequence was defined as this centre position ± 20 bp, then this window was extended further on both
524 sides by the length of the newly synthesised sequence. For example, if the newly synthesised sequence
525 was 10 bp centred on position #100, the search window was defined as the 61-bp sequence from
526 position #70 to #130 (10 bp—20 bp—centre position—20 bp—10 bp). We then detected the longest
527 common substring between the newly synthesised sequence and this search window using function
528 pmatchPattern from R package Biostrings. Polθ can also mediate insertions in reverse-complement
529 orientation [21] so we also searched for the longest common substring between the newly synthesised
530 sequence and the reverse-complement of the search window. From the longest common substring in
531 either direction, the algorithm kept the longest one then returned this substring if it was ≥6 bp. We
532 chose this 6-bp minimum length threshold because it brought down false-positive detections in the
533 simulated sample below 25%. This analysis only returned the longest continuous match ≥6 bp for each
534 insertion; therefore, other insertions or parts of an insertion may also be templated but may not be
535 detected as such. Similarly, the analysis was not designed to detect every Polθ-mediated insertion.
536 Polθ can also perform non-templated DNA synthesis [22] or use sequences far away (>250 bp) from the
537 cut as template [57].
538
539 As for the deletions, an insertion may match the neighbouring sequences by chance, and not because
540 these neighbouring sequences were genuinely used as template during DNA repair. To estimate these
541 null probabilities, we simulated 1000 newly synthesised sequences for each locus. To simulate each
542 newly synthesised sequence, we first drew a length from a distribution of newly synthesised sequence
543 lengths that is typical from repair of SpCas9 DSBs in zebrafish embryos (Supplementary Fig. 17b ; see
544 *Fitting distributions of deletion and insertion lengths*) and generated a random sequence (0.25
545 chance of each nucleotide) of this length. As for real insertions, we then detected whether ≥6 bp of this
546 random sequence matched neighbouring sequences, centring the search window on the cut position.
547
548 **Fitting distributions of deletion and insertion lengths**
549 To fit deletion and insertion lengths that are typical for repair of SpCas9 DSBs in zebrafish embryos
550 (Supplementary Fig. 17a,b), we collected sequencing reads from our previous work [50,58] totalling n =
551 191 embryos mutated across 38 loci using SpCas9 protein complexed with a synthetic
552 crRNA/tracrRNA duplex, for a total of 300,740 sequencing reads. Individual embryos were mutated
553 at 1–9 loci concomitantly but the amplicons were not sufficiently long to detect mutations spanning
554 multiple DSB sites. Reads were aligned with CRISPResso2 and mutations were called with CUTTER
555 (see *Sequencing analysis of prime-editing samples*).
556
557 For deletions, we only kept reads carrying some deletion(s) (200,065 reads), then excluded reads
558 carrying more than one deletions, which were 3218/200,065 (2%). To avoid extrapolating frequencies
559 from too few reads with a deletion, we excluded any sample with <100 reads with a deletion, leaving
560 155 samples across 35 loci. We then calculated, within each sample, the frequency of each unique
561 deletion (number of reads with the deletion/total number of reads with a deletion), then computed the
562 average frequency of each unique deletion across every sample (animal) from each locus, returning
563 one frequency for each indel at each locus. If a sample did not have a given deletion, we added a

frequency = 0 in the calculation. For example, if deletion X was only present as 5% of deletion reads in one of six samples from a given locus, we would calculate the average frequency of deletion X as the mean of 0.05, 0, 0, 0, 0, 0 (= 0.008). We then summed, for each locus, the frequencies of all deletions of the same length (e.g., sum of all 5-bp deletion frequencies at locus i), returning one frequency per deletion length at each locus. Finally, we computed the average frequency across loci of each deletion length, adding frequency = 0 each time a length was not found at a given locus. This estimated more general frequencies of each deletion length after repair of Cas9 DSBs in zebrafish embryos (e.g., overall frequency of 5-bp deletions). Supplementary Fig. 17a plots these frequencies, with sum of all frequencies = 1.0. The minimum deletion length was 1 bp, the maximum 74 bp, and the mode 3 bp. We tested various distributions offered by fitdistr from R package MASS to fit this distribution of deletion length frequencies. We chose a log-normal distribution based on visual assessment (Supplementary Fig. 17a) and because it gave a lower (i.e., better fit) D statistic than other distributions in a Kolmogorov–Smirnov test.

For insertions, we only kept reads carrying some insertion(s) (34,489 reads). If a read carried more than one insertions, we only considered one of the insertions, thus keeping the total number of insertion reads the same. To avoid extrapolating frequencies from too few reads with an insertion, we excluded any sample with <50 reads with an insertion, leaving 113 samples across 33 loci. Insertions in zebrafish often appear concomitantly with a multi-bp substitution (see example in Fig. 1k). For each insertion, we included any nearby substitution in the "newly synthesised sequence". Precisely, any substitution neighbouring the insertion was included in the newly synthesised sequence if it was separated from the insertion by ≤5 bp matching the reference (i.e., a substitution that was >5 bp away from the insertion was not included in the newly synthesised sequence). The following refers to the length of this newly synthesised sequence, rather than the length of the insertion directly. We calculated the average frequency of each length across samples and loci as for the deletions (see above). Supplementary Fig. 17b plots these frequencies, with sum of all frequencies = 1.0. The minimum newly synthesised sequence length was 1 bp, the maximum 95 bp, and the mode 1 bp. We tested various distributions offered by fitdistr from R package MASS to fit this distribution of length frequencies and chose an exponential distribution as it allowed to assign the highest frequency to the shortest length.

Machine learning pegRNA design tools

We collected edit rates for n = 39 pegRNAs tested in a PE2 RNP encoding 31 edits across 19 genomic loci: 32 pegRNAs from Petri et al., 2022 [3]; 6 from Vanhooydonck et al., 2025 [4]; and one from this study (*slc45a2* AA>GG).

For the sequencing data from Petri et al., 2022 [3], fastq files were downloaded as from NCBI Sequence Read Archive (SRA), BioProject #PRJNA713914 using fastq-dump from SRA Toolkit in command line. Reads were then processed and analysed using CRISPResso2 and CUTTER as for our sequencing data (see *Sequencing analysis of prime-editing samples*). PE3 and PE3b samples were excluded from our analyses. To test machine learning pegRNA design tools (see below), we calculated each sample's edit

rate as the sum of pure and impure edit proportions. To test the pegRNA design tools (Supplementary Fig. 6), we averaged edit/indel rates from all samples testing the same pegRNA, even if some experimental conditions varied (e.g., synthetic vs. in-vitro transcribed pegRNA; or incubation temperature after injection). Metadata were obtained from the authors' Supplementary Table 6 and 11.

Edit rates from Vanhooydonck et al., 2025 [4] were obtained from the authors' Supplementary Table 1. pegRNA sequences were obtained from Supplementary Table 5.

DeepPrime [14] offers 19 models, we excluded models trained for epegRNAs or NRCH PAM, leaving the 9 models listed in Supplementary Fig. 6c. DeepPrime only predicts pegRNAs for edits that are ≤3 bp. This left all pegRNAs encoding a substitution and one pegRNA from Petri et al., 2022 encoding a 3-bp insertion (*adgrf3b* 3-bp insertion), which we excluded as short insertions/deletions generally tend to give higher edit rates than substitutions in zebrafish, leaving n = 27 substitution-encoding pegRNAs to test the DeepPrime models. We obtained DeepPrime predictions for these pegRNAs using the .predict function from genet v0.17.1 Python library. PRIDICT v1 and v2 [18,19] pegRNA predictions were obtained using the website pridict.it/.

Base editing sequencing data from Rosello et al., 2022

Sequencing data from Rosello et al., 2022 [11] were downloaded as fastq files from NCBI SRA, BioProject #PRJNA825759 using fastq-dump from SRA Toolkit in command line. Metadata were from the authors' Supplementary Table 10. fastq files were processed and analysed using CUTTER as for our sequencing data (see *Sequencing analysis of prime-editing samples*), but without detection of scaffold incorporations. Samples plotted in Supplementary Fig. 11 are *tyr_5_50k.fastq* (Run #SRR18733203), *tyr_6_50k.fastq* (#SRR18733202), and *tyr_7_50k.fastq* (#SRR18733253).

Calculation of PBS:genome Tm

In Supplementary Fig. 6a, we used the R package rmelting to calculate the Tm of the PBS:genome duplex as in Ponnienselvan et al., 2023 [10]. For example, for the 7-nt PBS used in Supplementary Fig. 6b, the command was: melting(sequence="GGTCGTC", nucleic.acid.conc=2e-05, hybridisation.type='dnarna', Na.conc=1, method.nn ='sug95'). This command and examples were kindly provided to us by the authors.

***In-vitro* nickase assay**

To assess nickase activity of PEmax protein *in vitro*, we adapted the *in-vitro* prime editing experiment described by Anzalone et al., 2019 [7]. Fluorescently labelled DNA duplexes (sequences in Supplementary File 1) were produced by annealing two 5′-labelled oligonucleotides (IDT) corresponding to each of the complementary strand for the non-nicked substrate or three oligonucleotides for the pre-nicked substrate. RNPs were made of PEmax protein and gRNA (crRNA/tracrRNA duplex, IDT) complexed at a final concentration of 5 µM and incubated for 10 min at room temperature in 1× reaction buffer (20 mM HEPES pH 7.5; 100 mM KCl; 5% glycerol; 0.2 mM

EDTA pH 8.0; 3 mM MgCl2; 5 mM DTT). Next, duplex solution (0.4 µM final concentration) was added to the RNP solution. The reaction was incubated at 37°C for 1 hr. After successive RNase A and proteinase K treatments, the reaction was diluted in a formamide loading buffer (90% formamide, 10% glycerol, 0.01% bromophenol blue). The diluted reaction products were denatured at 95°C before being loaded into a denaturing urea polyacrylamide gel (8 M urea, 1× TBE, 15% polyacrylamide). The products were imaged using the BioRad ChemiDoc imaging system.

Acridine assay for detection of apoptotic cells

To stain apoptotic cells, we adapted the acridine orange staining assay described by Carrara et al., 2025 [5]. In the control experiment (Supplementary Fig. 16), wild-type embryos were collected and incubated at 28.5˚C. At 1 dpf, embryos were exposed to one of the following conditions: AOH1160 (MedChemExpress, 20 µM final concentration); $CdCl_2$ (Sigma-Aldrich, 20 µM final concentration); or 312–365 nm UV radiation. Note that cadmium ($CdCl_2$) is a toxic heavy metal, appropriate safety precautions must be put in place when resuspending the powder. For UV exposure, embryos were transferred to glass beakers and placed on a UV transilluminator used to cut bands from agarose gels (ECX-F20.SkyLight). UV was set to 100% and embryo were irradiated for 30 min. All embryos were then returned to the incubator. AOH1160 and $CdCl_2$ were washed-out the next morning (2 dpf, ~24 hr treatment) before acridine orange staining. In the *polq* mutant experiment (Fig. 2f), wild-type and *polq* mutant embryos were injected at the one-cell stage with PEmax RNPs carrying a targeting pegRNA (*slc45a2* GG>AA) or a pegRNA targeting a *BFP* transgene not present in these animals (sequence in Supplementary File 1), which served as non-targeting control for the effect of RNP injections. Acridine orange staining (see below) was then performed the next day at 1 dpf.

At 1 dpf (experiment with *polq* mutants) or 2 dpf (control experiment), embryos were pooled in groups of 20 and incubated in a 3 µg/mL acridine orange solution (Sigma-Aldrich) in egg medium for 30 min in the dark at room temperature. After staining, embryos were washed repeatedly in egg medium (without methylene blue) using a mini see-saw rocking shaker (100 oscillations/min), then transferred to fresh egg medium in a clean Petri dish. To facilitate imaging, embryos were manually dechorionated using fine forceps. Fluorescence imaging was performed using a Leica MSV269 microscope mounted with a Leica DFC310 FX camera. In the LAS X software, acquisition was set to black-and-white fluorescence mode. Acridine-positive cells exhibited green fluorescence (emission peak at 525 nm) when excited with a blue filter (excitation peak at 502 nm). The yolk tended to fluoresce brightly even after repeated wash-outs so we laid flat each larva as best as possible to focus the photograph on the tail. Images were analysed using Fiji v2.14.0 [59]. For each image, we segmented the tail region from the cloaca to the tail fin, set a minimum fluorescence intensity threshold to exclude background signal, and counted fluorescent puncta using Analyze > Analyze particles.

Images in Fig. 2f were acquired with an Olympus FV1000 laser scanning confocal microscope using a 20× 1.0 NA objective lens (Zeiss, W Plan-Apochromat 20×/1.0). Z-volumes were captured at a z-plane spacing of 3 µm; resolution was 1024 × 1024 pixels with a scan rate of 4 µs/pixel.

687 **Pictures**

688 For the pictures in Fig. 2g and Supplementary Fig. 10c, larvae were anaesthetised with tricaine (MS-
689 222) and pictures were taken with a Leica DFC310 FX camera mounted on a Leica MSV269 brightfield
690 microscope with illumination from below the sample.

691

692 **Variant types from ClinVar**

693 This refers to Supplementary Fig. 1. We downloaded file variant_summary.txt.gz from ClinVar's ftp
694 site in December 2024. We used variants on the GRCh38 (hg38) human genome reference, removed
695 duplicated variants, and only kept variants in protein-coding regions ("p." in variant name; e.g.,
696 "p.Gly262Arg"). The variants we labelled "premature stop" were those labelled as nonsense ("Ter" in
697 variant name; e.g., "p.Tyr47Ter") or frameshift ("fs" in variant name; e.g., "p.Phe468fs"). Category
698 "other" included the following types: "Indel", "Inversion", "Translocation", "Variation", "copy number
699 gain", "copy number loss", "Duplication", "Microsatellite".

700

701 **Statistics**

702 Threshold for statistical significance was 0.05. In figures, ns refers to $p > 0.05$, * to $p \leq 0.05$, ** to $p \leq$
703 0.01, *** to $p \leq 0.001$. In text, data distributions are reported as mean ± standard deviation, unless
704 stated otherwise.

705

706 **Software**

707 Data analysis was performed in R v4.4.2 ran through RStudio 2025.09.2+418; plots were generated
708 with R package ggplot2. Some analyses used Jupyter notebooks written in Python3. Figures were
709 prepared with Adobe Illustrator 2019.

710

711 **Data and data availability**

712 Source code of the CUTTER R package is available at github.com/francoiskroll/cutter.

713

714 Sequencing data will made available on NCBI SRA.

715

716 **Acknowledgements**

717 This work was supported by the Fondation pour la Recherche Médicale grant no. SPF202309017505
718 awarded to F.K and the European Commission HORIZON-PathFinder EdiGenT grant no. 101070903.

719

720 We thank the members of the Del Bene lab for helpful discussions. We thank Alexandra Lubin, Katie-
721 Jo Thorpe, and Tanvi Tambaki (Payne lab, UCL Cancer Institute, London) for the Illumina MiSeq
722 runs; Guillaume Pézeron (Muséum National d'Histoire Naturelle, Paris) for kindly giving access to his
723 microinjector and donating the *polq* KO line; Talya Goble and Jason Rihel (UCL, London) for
724 feedback on the draft manuscript.

725

Bibliography

1. Irion, U., Krauss, J. & Nüsslein-Volhard, C. Precise and efficient genome editing in zebrafish using the CRISPR/Cas9 system. *Development* **141**, 4827–4830 (2014).
2. Zu, Y. *et al.* TALEN-mediated precise genome modification by homologous recombination in zebrafish. *Nat. Methods* **10**, 329–331 (2013).
3. Petri, K. *et al.* CRISPR prime editing with ribonucleoprotein complexes in zebrafish and primary human cells. *Nat. Biotechnol.* **40**, 189–193 (2022).
4. Vanhooydonck, M. *et al.* Prime editing outperforms homology-directed repair as a tool for CRISPR-mediated variant knock-in in zebrafish. *Lab Anim.* **54**, 165–172 (2025).
5. Carrara, M. *et al.* Dynamic interplay of cNHEJ and MMEJ pathways of DNA double-strand break repair during embryonic development in zebrafish. *Sci. Rep.* **15**, 4886 (2025).
6. Thyme, S. B. & Schier, A. F. Polq-Mediated End Joining Is Essential for Surviving DNA Double-Strand Breaks during Early Zebrafish Development. *Cell Rep.* **15**, 707–714 (2016).
7. Anzalone, A. V. *et al.* Search-and-replace genome editing without double-strand breaks or donor DNA. *Nature* **576**, 149–157 (2019).
8. Liu, P. *et al.* Increasing intracellular dNTP levels improves prime editing efficiency. *Nat. Biotechnol.* **43**, 539–544 (2025).
9. Ono, Y. *et al.* Optimised genome editing for precise DNA insertion and substitution using Prime Editors in zebrafish. *eLife* **14**, (2025).
10. Ponnienselvan, K. *et al.* Reducing the inherent auto-inhibitory interaction within the pegRNA enhances prime editing efficiency. *Nucleic Acids Res.* **51**, 6966–6980 (2023).
11. Rosello, M. *et al.* Disease modeling by efficient genome editing using a near PAM-less base editor in vivo. *Nat. Commun.* **13**, 3435 (2022).
12. Streisinger, G., Singer, F., Walker, C., Knauber, D. & Dower, N. Segregation analyses and gene-centromere distances in zebrafish. *Genetics* **112**, 311–319 (1986).
13. Dang, Y. *et al.* Optimizing sgRNA structure to improve CRISPR-Cas9 knockout efficiency. *Genome Biol.* **16**, 280 (2015).
14. Yu, G. *et al.* Prediction of efficiencies for diverse prime editing systems in multiple cell types. *Cell* **186**, 2256-2272.e23 (2023).
15. Yan, J. *et al.* Improving prime editing with an endogenous small RNA-binding protein. *Nature* **628**, 639–647 (2024).
16. Nelson, J. W. *et al.* Engineered pegRNAs improve prime editing efficiency. *Nat. Biotechnol.* **40**, (2022).
17. Antoniou, P. *et al.* Modified pegRNAs mitigate scaffold-derived prime editing by-products. *Nat. Commun.* **16**, 3374 (2025).
18. Mathis, N. *et al.* Machine learning prediction of prime editing efficiency across diverse chromatin contexts. *Nat. Biotechnol.* **43**, (2025).
19. Mathis, N. *et al.* Predicting prime editing efficiency and product purity by deep learning. *Nat. Biotechnol.* **41**, (2023).
20. Schimmel, J., Kool, H., van Schendel, R. & Tijsterman, M. Mutational signatures of non-homologous and polymerase theta-mediated end-joining in embryonic stem cells. *EMBO J.* **36**, 3634–3649 (2017).
21. Schimmel, J., van Schendel, R., den Dunnen, J. T. & Tijsterman, M. Templated Insertions: A Smoking Gun for Polymerase Theta-Mediated End Joining. *Trends Genet. TIG* **35**, 632–644 (2019).
22. Kent, T., Mateos-Gomez, P. A., Sfeir, A. & Pomerantz, R. T. Polymerase θ is a robust terminal transferase that oscillates between three different mechanisms during end-joining. *eLife* **5**, e13740 (2016).
23. Lee, J. *et al.* Prime editing with genuine Cas9 nickases minimizes unwanted indels. *Nat. Commun.* **14**, 1786 (2023).
24. Kelsh, R. N. *et al.* Zebrafish pigmentation mutations and the processes of neural crest development. *Dev. Camb. Engl.* **123**, 369–389 (1996).
25. Rees, H. A., Yeh, W.-H. & Liu, D. R. Development of hRad51–Cas9 nickase fusions that mediate HDR without double-stranded breaks. *Nat. Commun.* **10**, 2212 (2019).
26. Koblan, L. W. *et al.* Improving cytidine and adenine base editors by expression optimization and ancestral reconstruction. *Nat. Biotechnol.* **36**, 843–846 (2018).
27. Chauhan, V. P., Sharp, P. A. & Langer, R. Engineered prime editors with minimal genomic errors. *Nature* **646**, 1254–1260 (2025).
28. Kimble, M. T. *et al.* Repair of replication-dependent double-strand breaks differs between the leading and lagging strands. *Mol. Cell* **85**, 61-77.e6 (2025).
29. Kuzminov, A. Single-strand interruptions in replicating chromosomes cause double-strand breaks. *Proc. Natl. Acad. Sci. U. S. A.* **98**, 8241–8246 (2001).
30. Pavani, R. *et al.* Structure and repair of replication-coupled DNA breaks. *Science* **385**, eado3867 (2024).
31. Vrtis, K. B. *et al.* Single-strand DNA breaks cause replisome disassembly. *Mol. Cell* **81**, 1309-1318.e6 (2021).
32. Xu, Y. *et al.* DNA nicks in both leading and lagging strand templates can trigger break-induced replication. *Mol. Cell* **85**, 91-106.e5 (2025).
33. Kane, D. A. & Kimmel, C. B. The zebrafish midblastula transition. *Dev. Camb. Engl.* **119**, 447–456 (1993).
34. Kimmel, C. B., Ballard, W. W., Kimmel, S. R., Ullmann, B. & Schilling, T. F. Stages of embryonic development of the zebrafish. *Dev. Dyn.* **203**, 253–310 (1995).
35. Olivier, N. *et al.* Cell lineage reconstruction of early zebrafish embryos using label-free nonlinear microscopy. *Science* **329**, 967–971 (2010).
36. Siefert, J. C., Clowdus, E. A. & Sansam, C. L. Cell Cycle Control in the Early Embryonic Development of Aquatic Animal Species. *Comp. Biochem. Physiol. Toxicol. Pharmacol. CBP* **178**, 8–15 (2015).
37. Koblan, L. W. *et al.* High-resolution spatial mapping of cell state and lineage dynamics in vivo with PEtracer. *Science* **390**, eadx3800 (2025).
38. Kim-Yip, R. P. *et al.* Efficient prime editing in two-cell mouse embryos using PEmbryo. *Nat. Biotechnol.* **42**, 1822–1830 (2024).
39. Davis, L. & Maizels, N. Homology-directed repair of DNA nicks via pathways distinct from canonical double-strand break repair. *Proc. Natl. Acad. Sci. U. S. A.* **111**, E924-932 (2014).
40. Bao, Z., Zhao, Z., Boyle, T. J., Murray, J. I. & Waterston, R. H. Control of Cell Cycle Timing during C. elegans Embryogenesis. *Dev. Biol.* **318**, 65–72 (2008).
41. Tsai, T. Y.-C., Theriot, J. A. & Jr, J. E. F. Changes in Oscillatory Dynamics in the Cell Cycle of Early Xenopus laevis Embryos. *PLOS Biol.* **12**, e1001788 (2014).

42. Yuan, K., Seller, C. A., Shermoen, A. W. & O'Farrell, P. H. Timing the Drosophila Mid-Blastula Transition: a cell cycle-centered view. *Trends Genet. TIG* **32**, 496–507 (2016).
43. Deng, L. *et al.* Mitotic CDK Promotes Replisome Disassembly, Fork Breakage, and Complex DNA Rearrangements. *Mol. Cell* **73**, 915-929.e6 (2019).
44. Hanscom, T. *et al.* Characterization of sequence contexts that favor alternative end joining at Cas9-induced double-strand breaks. *Nucleic Acids Res.* **50**, 7465–7478 (2022).
45. Roerink, S. F., van Schendel, R. & Tijsterman, M. Polymerase theta-mediated end joining of replication-associated DNA breaks in C. elegans. *Genome Res.* **24**, 954–962 (2014).
46. Hu, M. *et al.* Scalable modulation of CRISPR–Cas enzyme activity using photocleavable phosphorothioate DNA. *Nat. Commun.* **16**, 5939 (2025).
47. Biggin, M. D. Animal Transcription Networks as Highly Connected, Quantitative Continua. *Dev. Cell* **21**, 611–626 (2011).
48. Ménoret, S. *et al.* Homology-directed repair in rodent zygotes using Cas9 and TALEN engineered proteins. *Sci. Rep.* **5**, 14410 (2015).
49. Chen, P. J. *et al.* Enhanced prime editing systems by manipulating cellular determinants of editing outcomes. *Cell* **184**, 5635-5652.e29 (2021).
50. Kroll, F. *et al.* A simple and effective F0 knockout method for rapid screening of behaviour and other complex phenotypes. *eLife* **10**, e59683 (2021).
51. Redmon, J., Divvala, S., Girshick, R. & Farhadi, A. You Only Look Once: Unified, Real-Time Object Detection. in 779–788 (2016).
52. Hwang, G.-H. *et al.* Analyzing long-read CRISPR experiments with CRISPRLungo. 2025.10.21.683786 Preprint at https://doi.org/10.1101/2025.10.21.683786 (2025).
53. Meeker, N. D., Hutchinson, S. A., Ho, L. & Trede, N. S. Method for isolation of PCR-ready genomic DNA from zebrafish tissues. *BioTechniques* **43**, 610, 612, 614 (2007).
54. Li, H. *et al.* The Sequence Alignment/Map format and SAMtools. *Bioinformatics* **25**, 2078–2079 (2009).
55. Quinlan, A. R. & Hall, I. M. BEDTools: a flexible suite of utilities for comparing genomic features. *Bioinformatics* **26**, 841–842 (2010).
56. Clement, K. *et al.* CRISPResso2 provides accurate and rapid genome editing sequence analysis. *Nat. Biotechnol.* **37**, 224–226 (2019).
57. Schimmel, J., Kool, H., van Schendel, R. & Tijsterman, M. Mutational signatures of non-homologous and polymerase theta-mediated end-joining in embryonic stem cells. *EMBO J.* **36**, 3634–3649 (2017).
58. Kroll, F., Donnelly, J., Özcan, G. G., Mackay, E. & Rihel, J. Behavioural pharmacology predicts disrupted signalling pathways and candidate therapeutics from zebrafish mutants of Alzheimer's disease risk genes. *eLife* **13**, RP96839 (2025).
59. Schindelin, J. *et al.* Fiji: an open-source platform for biological-image analysis. *Nat. Methods* **9**, 676–682 (2012).
60. Terzioglu, M., Saralahti, A., Piippo, H., Rämet, M. & Andressoo, J.-O. Improving CRISPR/Cas9 mutagenesis efficiency by delaying the early development of zebrafish embryos. *Sci. Rep.* **10**, 21023 (2020).
61. Oscorbin, I. P. & Filipenko, M. L. M-MuLV reverse transcriptase: Selected properties and improved mutants. *Comput. Struct. Biotechnol. J.* **19**, 6315–6327 (2021).
62. Walton, R. T., Christie, K. A., Whittaker, M. N. & Kleinstiver, B. P. Unconstrained genome targeting with near-PAMless engineered CRISPR-Cas9 variants. *Science* **368**, 290–296 (2020).

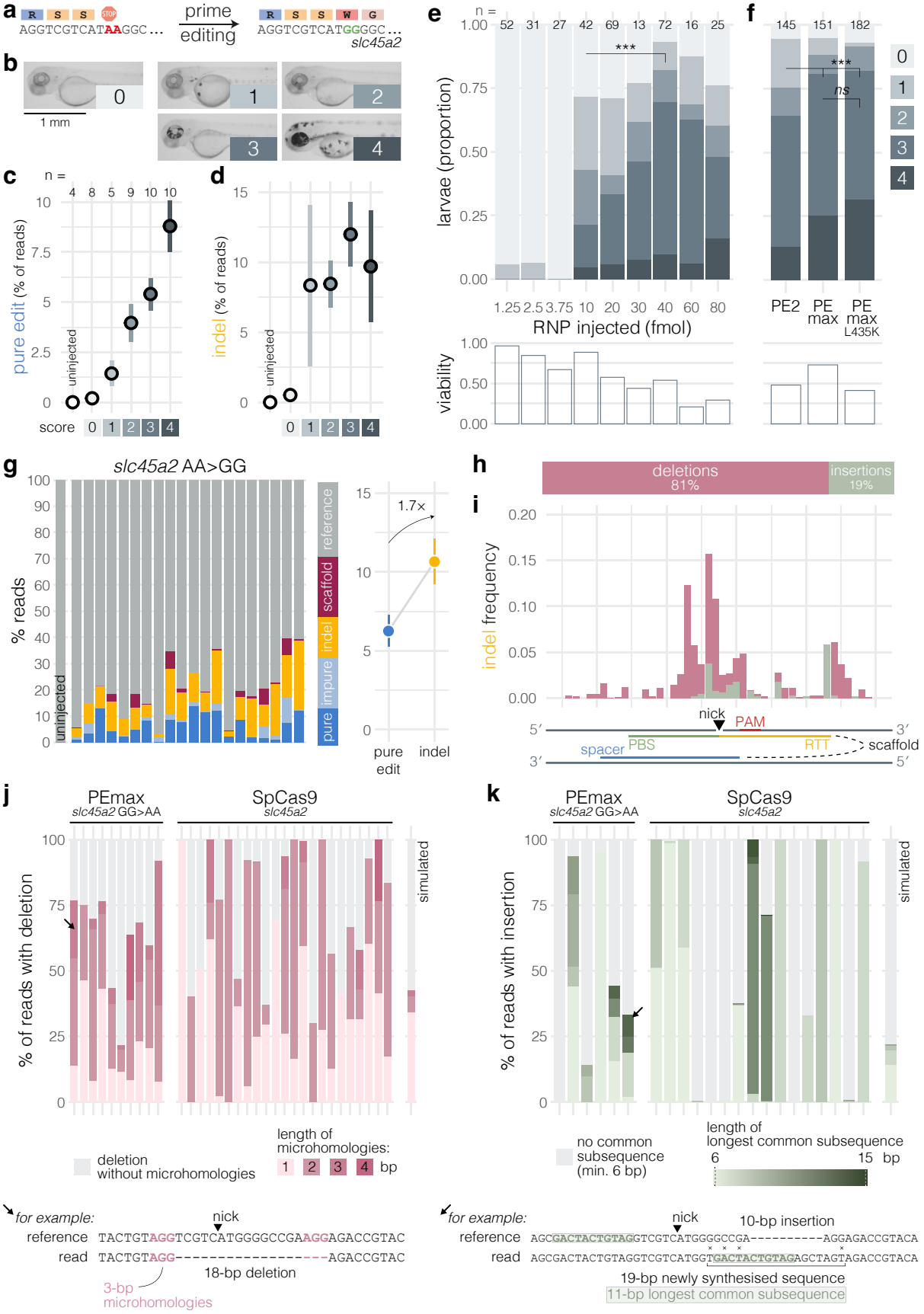

FIGURE 1

Figure 1 | Indels generated during prime editing in zebrafish show signature of microhomology-mediated end-joining.

a, Prime editing was used to create a two-nucleotide substitution in the pigmentation gene *slc45a2*, reverting a premature stop codon (TAA) back into the wild-type tryptophan codon (TGG).
b, Pictures of 3-dpf *slc45a2*^{W121*} homozygous larvae injected with PE2/pegRNA RNP as examples of the pigmentation scoring method.
c, Pure edit rates (% of reads, mean ± SEM) of larvae assigned to each pigmentation score.
d, Indel rates (% of reads, mean ± SEM) of larvae assigned to each pigmentation score.
e, (top) Phenotypic penetrance (proportion of larvae assigned to each pigmentation score) when gradually more PE2/pegRNA RNP was injected at the 1:1 ratio. Doses ≥10 fmol generally correlated with higher rates of pigmented larvae, in line with a previous report [8]. 10 vs. 40 fmol: *** $p < 0.001$ by Fisher's exact test. (bottom) Viability as proportion of larvae assessed as viable at 3 dpf, normalised to uninjected embryos. Doses >40 fmol lowered viability without further increasing rates of pigmented larvae.
f, (top) Phenotypic penetrance (pigmentation scores) in larvae injected with 30 fmol of PE2, PEmax [49], or PEmax^{L435K} RNP [8]. Compared to PE2, PEmax and PEmax^{L435K} both increased 1.3-fold the proportion of highly pigmented larvae (scores 3 and 4). ns $p = 0.11$, *** $p < 0.001$ by Fisher's exact test. (bottom) Viability as proportion of larvae assessed as viable at 3 dpf, normalised to uninjected embryos.
g, (left) Sequencing results from larvae injected with PE2/pegRNA RNP. Each bar represents an individual larva, with colours representing the percentage of reads assigned to each label. Four samples with <10 modified reads were excluded. Minimum sequencing depth was 1377×. n = 20 injected samples. (right) The pure edit rate compared to the indel rate (mean ± SEM).
h, In the average *slc45a2* AA>GG prime-edited sample, 83% of reads with an indel had a deletion, the other 17% had an insertion.
i, Frequency of prime editing-generated indels across genomic positions at the *slc45a2* locus. Samples included were larvae injected with the *slc45a2* AA>GG pegRNA complexed with PE2 or PEmax protein, for a total of n = 31 samples. Each frequency represents the average frequency across larvae of indels starting at this position. Each indel (n = 343 unique indels observed) contributes to the frequency once at its start position, which is the most 5′ nucleotide involved. For example, a 10-bp deletion which deleted nucleotide #90–99 is counted at #90. Scaffold incorporations are not included.
j, (top) Of all sequencing reads with a deletion, percentage which showed microhomologies flanking the deletion. Each bar represents an individual larva injected with PEmax or SpCas9 RNP targeting the *slc45a2* locus. Darker pink colours represent longer microhomologies, grey represents deletions without microhomologies. There were 36–8030 reads with a deletion per larva. The "simulated" sample represents 1000 simulated deletions. (bottom) Example of an 18-bp deletion flanked by 3-bp microhomologies; the arrow indicates the sample in which it was found.
k, (top) Of all sequencing reads with an insertion, percentage which had a ≥6 bp continuous match between the "newly synthesised sequence" and the neighbouring sequences. Insertions generated during DSB repair in zebrafish are often accompanied with a multi-bp substitution (see example at bottom), they together form the "newly synthesised sequence" which is compared to the neighbouring sequences to find a possible match. Darker green colours represent longer matches between the newly synthesised sequence and the neighbouring sequences, grey represents newly synthesised sequences

with a <6 bp match; that is, whose length was too short to analyse, or were untemplated, or used a template that was further away. There were 45–2866 reads with an insertion per larva. The "simulated" sample represents 1000 newly synthesised sequences generated at random. (bottom) Example of a 19-bp newly synthesised sequence with at least 11 bp templated from a neighbouring sequence (green); the arrow indicates the sample in which it was found.

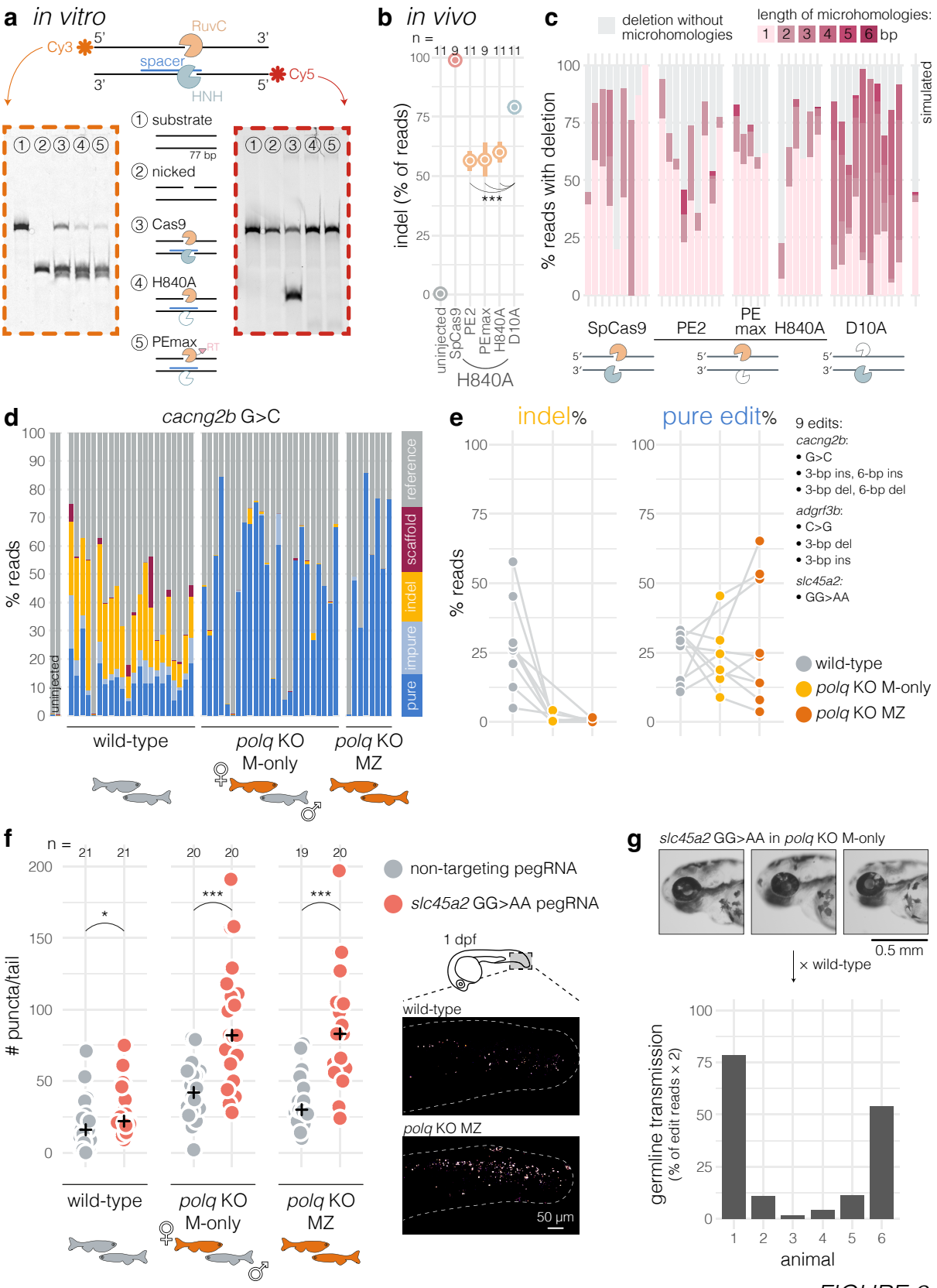

FIGURE 2

Figure 2 | Prime editing in absence of maternally-deposited Polθ achieves near-perfect precision.

a, SpCas9 has two nuclease domains: the HNH domain cuts the target strand (strand to which the gRNA is annealed) and the RuvC domain cuts the opposite non-target strand. Here, *in-vitro* cleavage

of a fluorescently-labelled double-stranded DNA substrate encoding a portion of *BFP* by SpCas9, H840A nickase, or PEmax, followed by denaturing PAGE. (left) Gel illuminated to detect Cy3 fluorescence emitted from the 5′–3′ forward strand. (right) Gel illuminated to detect Cy5 fluorescence emitted from the 3′–5′ reverse strand.

b, Indel rates (% of reads, mean ± SEM) of larvae injected with RNP made of each protein and a gRNA targeting *tyr*. D10A vs. PE2 or PEmax or H840A: *** $p < 0.001$ by Welch's t-tests.

c, Of all sequencing reads with a deletion, percentage which showed microhomologies flanking the deletion. Each bar represents an individual larva. Darker pink colours represent longer microhomologies, grey represents deletions without microhomologies. There were 50–735 reads with a deletion per larva. The "simulated" sample represents 1000 simulated deletions.

d, Sequencing results from wild-type, *polq* maternal-only heterozygous KO, and *polq* maternal-zygotic homozygous KO larvae uninjected or injected with PEmax complexed with a pegRNA encoding a one-bp substitution (G>C) in *cacng2b*. Each bar represents an individual larva, with colours representing the percentage of reads assigned to each label. Cartoons below represent the parental crosses that generated the injected embryos; orange fish are homozygous *polq* KO. Minimum sequencing depth was 60×. n = 54 injected samples. KO, knockout; M-only, maternal-only; MZ, maternal-zygotic.

e, Each datapoint represents the average indel (left) or pure edit (right) rate (% of reads) of 7–24 larvae of same genotype (wild-type, *polq* maternal-only heterozygous KO, or *polq* maternal-zygotic homozygous KO) and injected with the same pegRNA. Lines connect datapoints from the same pegRNA. n = 9 pegRNAs (7 for maternal-only *polq* KO; *adgrf3b* 3-bp insertion and *cacng2b* 6-bp deletion are missing); n = 278 injected samples in total.

f, Detection of apoptotic cells using acridine orange staining. (left) Each datapoint represents the number of acridine-positive puncta in the tail of an individual 1-dpf wild-type, *polq* maternal-only heterozygous KO, or *polq* maternal-zygotic homozygous KO embryo injected with PEmax complexed with a non-targeting pegRNA or the *slc45a2* GG>AA pegRNA. Black crosses mark the group medians. Cartoons below represent the parental crosses that generated the injected embryos; orange fish are homozygous *polq* KO. * $p = 0.011$, *** $p < 0.001$ by Mann-Whitney U tests. (right) Example images of the tail of a 1-dpf wild-type or *polq* maternal-zygotic homozygous KO embryo injected with the *slc45a2* GG>AA pegRNA showing acridine orange-positive puncta.

g, (top) Example pictures of 3-dpf *polq* maternal-only heterozygous KO larvae injected with PEmax^{L435K}/*slc45a2* GG>AA pegRNA that were selected to be grown because they had patches of eye depigmentation. (bottom) Germline transmission rates of the *slc45a2* GG>AA edit measured from six F1 clutches. Minimum sequencing depth was 2283×.

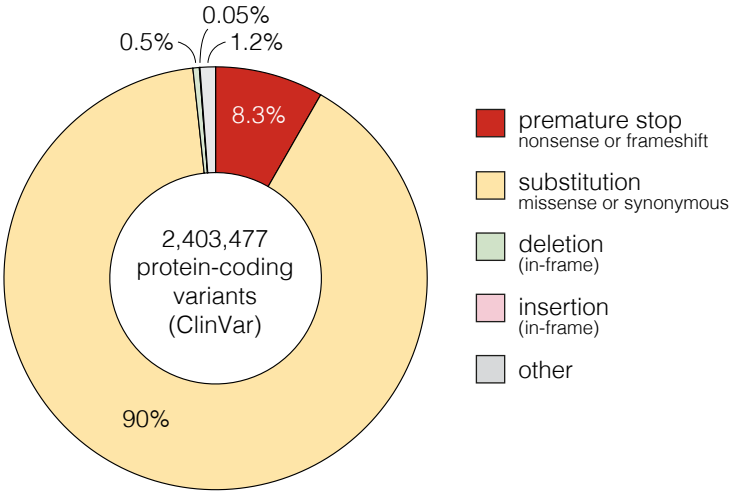

Supplementary Figure 1

Supplementary Fig. 1 | Types of human variants recorded in ClinVar.
Proportions of different types of human genomic variants recorded in the ClinVar database. Only variants in protein-coding sequences were included.

Supplementary Fig. 2 | Development of the pigmentation recovery assay for quick readout of prime editing rates.

a, Sequencing results from larvae grouped according to their pigmentation score. Each bar represents an individual larva, with colours representing the percentage of reads assigned to each label, see b. Minimum sequencing depth was 131×. n = 42 injected samples.

b, Examples of sequencing reads. Every read is assigned a single label depending on its mutation calls: “reference” if the read matches the reference sequence; “pure edit” if only the expected edit (AA>GG) is present; “impure edit” if the expected edit and one or more indel(s) are present; “indel” if the read does not carry the edit but one or more indels; and “scaffold” if a sequence likely templated from the pegRNA’s scaffold is present.

c, Scaffold incorporations can include both substitutions and insertions. (top) Of 1274 reads with a scaffold incorporation from the *slc45a2* prime-edited samples in Supplementary Fig. 5c, 1170 (92%) had a scaffold substitution (orange), 104 (8%) had a scaffold insertion (khaki). (bottom) Examples of reads with a scaffold incorporation. sub, substitution; ins, insertion.

d, Concordance in pigmentation scores between two scorers assessing the same injected larvae. Colours in each bar plot represent the proportion of larvae assigned to each pigmentation score.

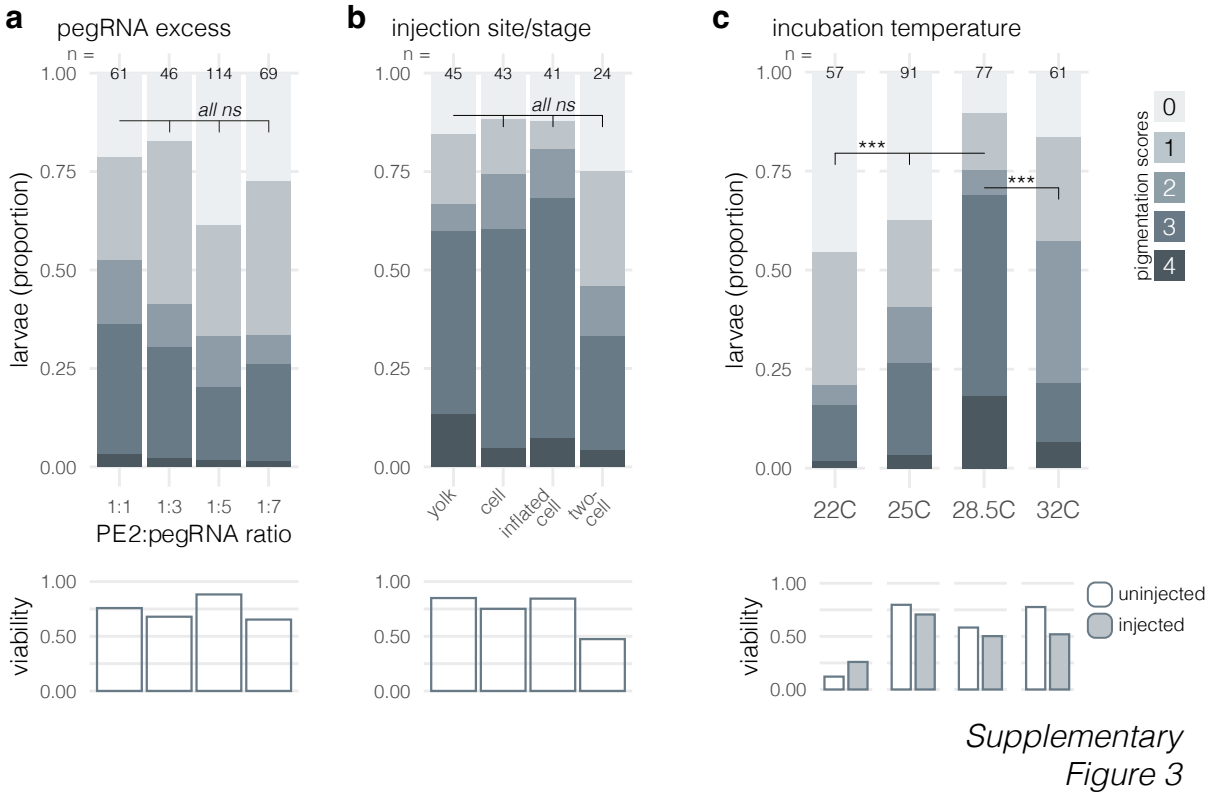

Supplementary Fig. 3 | Optimisation of PE RNP injection conditions using the pigmentation recovery assay.

a, As the pegRNA PBS is fully complementary to the spacer, the pegRNA may misfold, blocking its activity [10]. Using an excess of pegRNA could benefit prime editing rates by providing the PE protein with more correctly folded pegRNA. (top) Here, phenotypic penetrance (proportion of larvae assigned to each pigmentation score) when an excess of pegRNA was used. PE2 protein was kept constant at 26 fmol while pegRNA was gradually increased. 1:1: 26 fmol, 1:3: 78 fmol, 1:5: 130 fmol, 1:7: 182 fmol pegRNA. ns $p > 0.07$ by Fisher's exact test. (bottom) Viability as proportion of larvae assessed as viable at 6 dpf, normalised to uninjected embryos.

b, Solution can be injected in the zebrafish egg's yolk or cell. Yolk injections are quicker but the RNP must first cross into the cell. Cell injection may be beneficial by avoiding this delay. In mouse zygotes, injections at the two-cell stage increased edit rates [38]. (top) Here, phenotypic penetrance (pigmentation scores) depending on injection site. Embryos were injected with 30 fmol (1 nL) of PE2/pegRNA RNP, except two-cell stage embryos which received 30 fmol (1 nL) of RNP in each cell, so 60 fmol (2 nL) total. ns $p > 0.32$ by Fisher's exact test. (bottom) Viability as proportion of larvae assessed as viable at 5 dpf, normalised to uninjected embryos.

c, The standard incubation temperature for zebrafish embryos is 28.5˚C but as ectotherms can develop in a range of temperatures. Cooler incubation temperatures likely benefit Cas9 nuclease mutagenesis by delaying the first divisions [60]. In contrast, warmer incubation at 32˚C increased prime editing rates in a previous zebrafish study [3], potentially because this is closer to the optimal temperature of the RT [61]. (top) Here, phenotypic penetrance (pigmentation scores) after incubation at different temperatures. Embryos were incubated for 3 hr directly after injection at the corresponding

temperature then transferred to 28.5˚C. *** $p < 0.001$ by Fisher's exact test. (bottom) Viability as proportion of larvae assessed as viable at 6 dpf. We also tested 18˚C but too few embryos survived (6/136).

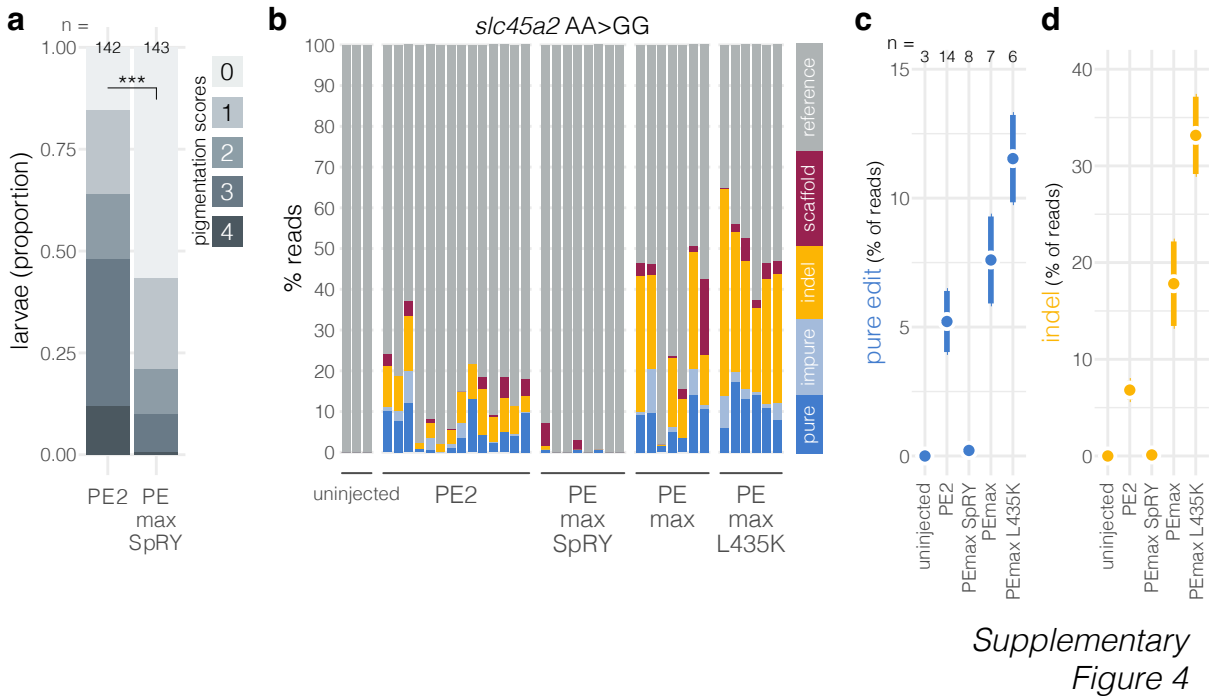

Supplementary Figure 4

Supplementary Fig. 4 | Test of PE protein variants at *slc45a2* AA>GG.

a, PEmax SpRY uses a Cas9 variant that recognises any NRN PAM (R = G or A) instead of the standard NGG PAM [62]. Here, phenotypic penetrance (proportion of larvae assigned to each pigmentation score) in larvae injected with 30 fmol of PE2 or PEmax SpRY complexed with pegRNA. Compared to PE2, PEmax SpRY reduced 5-fold (48 to 10%) the frequency of highly pigmented larvae (scores 3 and 4). *** $p < 0.001$ by Fisher's exact test.

b, Sequencing results from larvae injected with 30 fmol of the corresponding PE RNP. Each bar represents an individual larva, with colours representing the percentage of reads assigned to each label. Minimum sequencing depth was 766×. n = 35 injected samples.

c, Pure edit rates (% of reads, mean ± SEM) of larvae injected with each PE RNP.

d, Indel rates (% of reads, mean ± SEM) of larvae injected with each PE RNP.

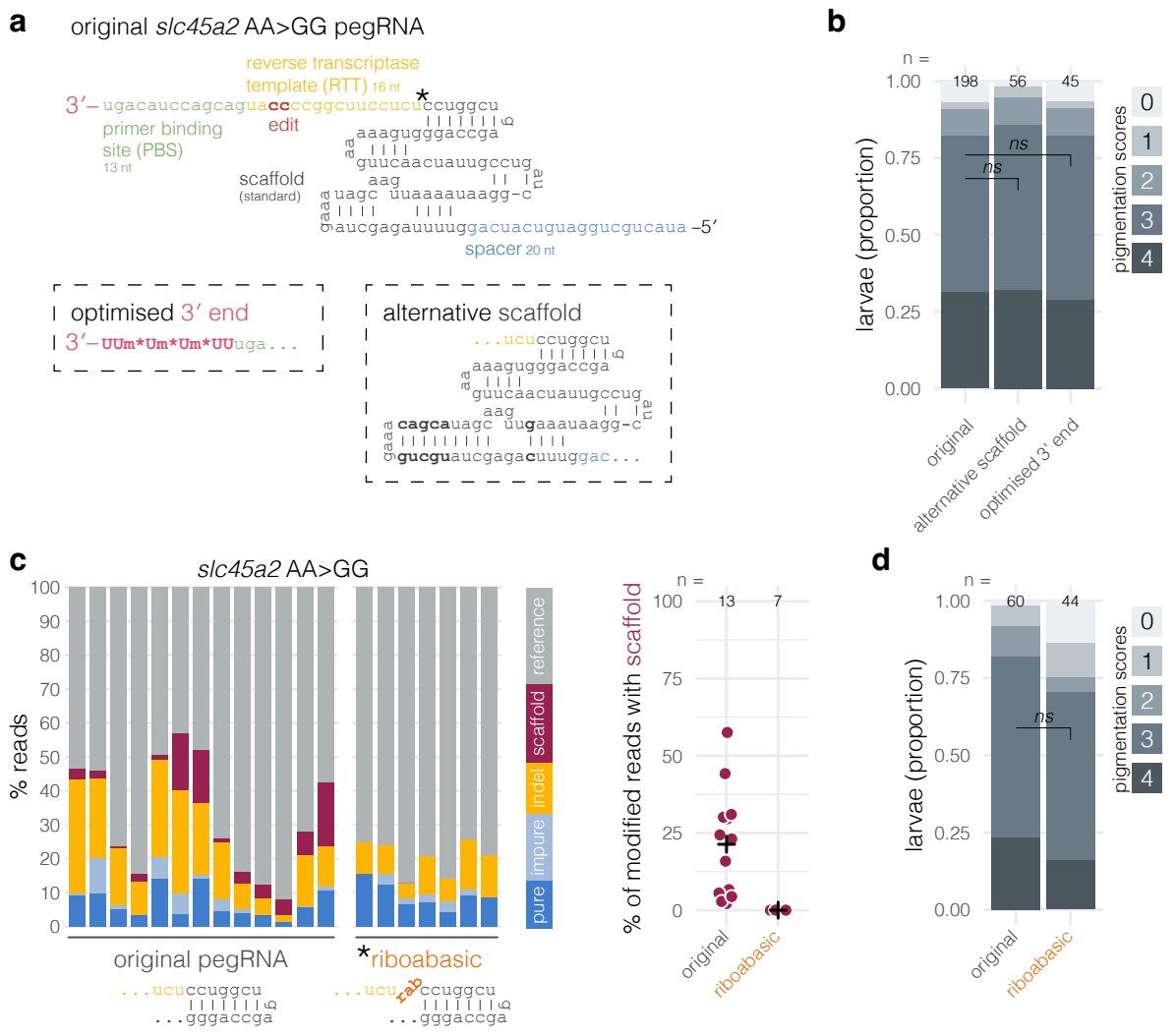

Supplementary Figure 5

Supplementary Fig. 5 | Test of pegRNA modifications at *slc45a2* GG>AA.

a, The full sequence of the original *slc45a2* pegRNA used in the pigmentation recovery assay. (bottom left) The pegRNA's 3′ end (PBS side) protrudes outside of the RNP, exposing it to exonuclease activity [16]. Here, the chemically modified 3′-end from Yan et al., 2024 optimised to protect the pegRNA end while also allowing the binding of La, an endogenous RNA-binding protein found to enhance prime editing [15]. Um denotes a uridine carrying a 2′-O-methylation; * denotes a phosphorothioate bond. (bottom right) The alternative pegRNA scaffold from Dang et al., 2015 found to increase prime editing activity by 1.25-fold in HEK293T cells [13,14]. Compared to the standard scaffold, the tetraloop is extended by 5 nt and a uridine in a four-uridine stretch is substituted to cytidine (nucleotides in bold).

b, Phenotypic penetrance (proportion of larvae assigned to each pigmentation score) in larvae injected with 30 fmol of PEmax^{L435K} complexed with the original *slc45a2* AA>GG pegRNA, or the alternative scaffold pegRNA, or the optimised 3′-end pegRNA. ns $p > 0.6$ by Fisher's exact test.

c, (left) Sequencing results from larvae injected with 30 fmol PEmax complexed with the original *slc45a2* pegRNA or with the same pegRNA but carrying a riboabasic spacer (rab) between the RTT and the scaffold. Each bar represents an individual larva, with colours representing the percentage of

reads assigned to each label. (right) Each larva's scaffold incorporation rate as percentage of all modified reads (any read that is not reference). Black crosses mark the group means. Minimum sequencing depth was 364×. n = 20 samples. The original pegRNA group includes five PEmax samples also plotted in Supplementary Fig. 4b. Samples with <50 modified reads were excluded to calculate scaffold incorporation rates from a representative number of modified reads.

d, Phenotypic penetrance (pigmentation scores) in larvae injected with PEmax RNP carrying the original *slc45a2* pegRNA or the riboabasic spacer pegRNA, as in c. ns p = 0.11 by Fisher's exact test.

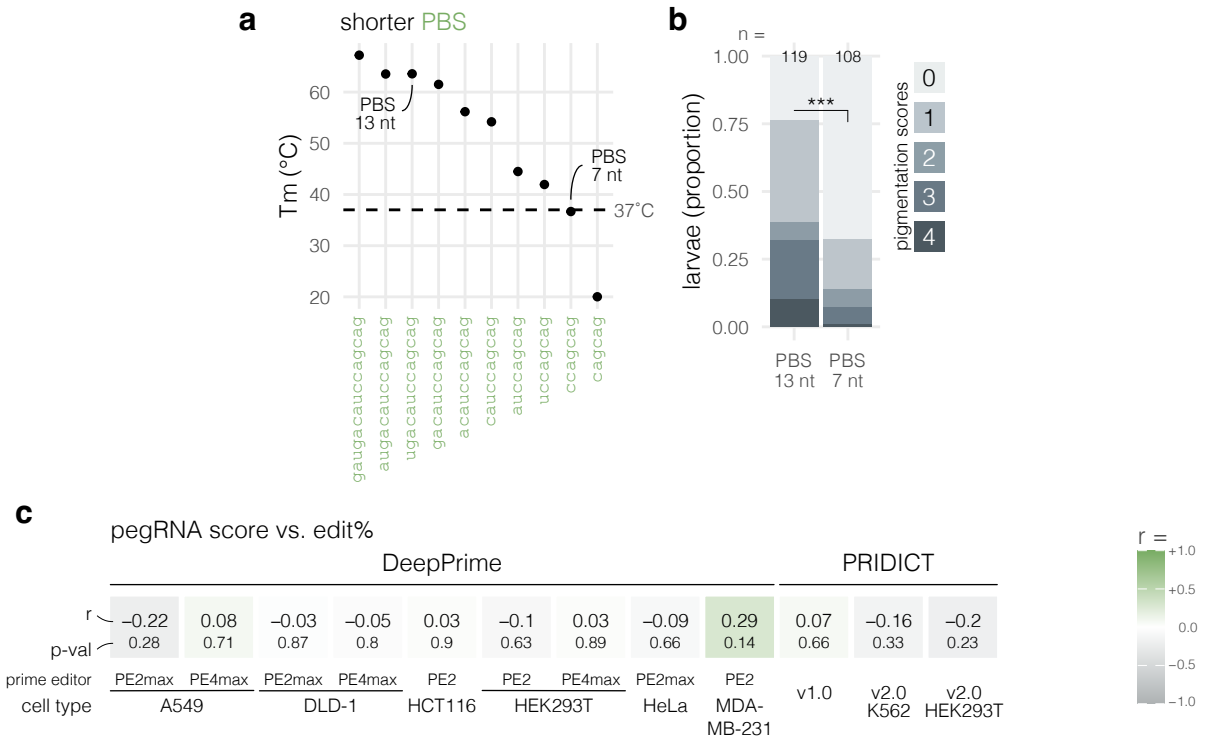

Supplementary Figure 6

Supplementary Fig. 6 | Assessment of pegRNA design tools in zebrafish embryos.

a, Tm calculations of the PBS:genome duplex as the PBS of the *slc45a2* AA>GG pegRNA is shortened from 15 to 6 nt.

b, Phenotypic penetrance (proportion of larvae assigned to each pigmentation score) in larvae injected with 30 fmol of PE2 protein complexed with the original 13-nt PBS *slc45a2* AA>GG pegRNA or its 7-nt PBS counterpart. *** $p < 0.001$ by Fisher's exact test.

c, Predictions of pegRNA editing efficiencies in zebrafish embryos by 12 machine learning models. Tile colour represents Pearson's correlations (r from −1 to +1). In each tile, the top number is Pearson's r, the bottom is its p-value. The correlation is calculated between the pegRNAs' predicted scores and their average edit rates (sum of pure and impure edit rates) in zebrafish embryos. Median number of samples per pegRNA was 5. For PRIDICT [18,19]: n = 39 pegRNAs, which is the complete dataset. DeepPrime [14] only works on edits ≤3 bp so not every pegRNA could be included: n = 27 pegRNAs. Including only the substitution-encoding pegRNAs (same set as for DeepPrime) in the PRIDICT analysis did not change the interpretation (r = −0.28 to −0.08). We also tested the correlation between the pegRNAs' "unintended scores" predicted by PRIDICT v1 and their average indel rates: r = −0.04, p = 0.8. Data from Petri et al., 2022 (n = 32 pegRNAs); Vanhooydonck et al., 2025 (n = 6 pegRNAs); and the *slc45a2* AA>GG used with PE2 RNP in this study. Embryos were injected with ~6 fmol (30 fmol for *slc45a2* AA>GG) of RNP made of PE2 protein and *in-vitro* transcribed or synthetic pegRNA.

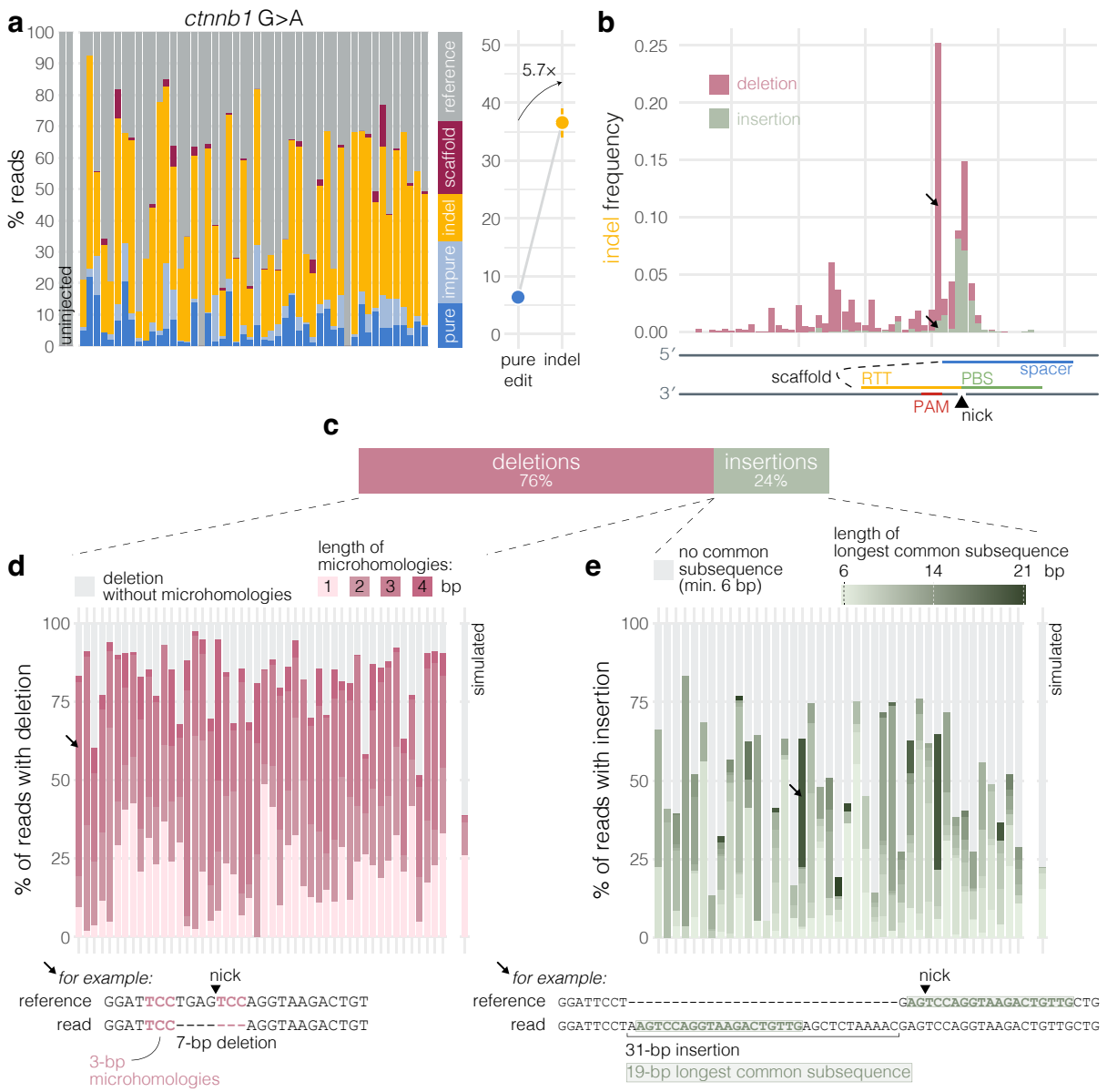

Supplementary Figure 7

Supplementary Fig. 7 | Indels generated during prime editing at *ctnnb1* show signatures of MMEJ.

a, (left) Sequencing results from larvae injected with 30 fmol PEmax complexed with pegRNA encoding a one-bp substitution (G>A) in *ctnnb1*. Each bar represents an individual larva, with colours representing the percentage of reads assigned to each label. Minimum sequencing depth was 456×. n = 60 injected samples. (right) The pure edit rate compared to the indel rate (mean ± SEM).

b, Frequency of prime editing-generated indels across genomic positions at the *ctnnb1* locus, from n = 48 of the samples in a. Each frequency represents the average frequency across larvae of indels starting at this position. Each indel (n = 639 unique indels observed) contributes to the frequency once at its start position, which is the most 5′ nucleotide involved. For example, a 7-bp deletion which deleted nucleotide #71–77 is counted at #71. Scaffold incorporations are not included.

c, In the average *ctnnb1* prime-edited sample, 76% of reads with an indel had a deletion, the other 24% had an insertion.

d, (top) Of all sequencing reads with a deletion, percentage which showed microhomologies flanking the deletion. Each bar represents an individual prime-edited larva. Darker pink colours represent longer microhomologies, grey represents deletions without microhomologies. There were 102–1561 reads with a deletion per larva. n = 48 samples. The "simulated" sample represents 1000 simulated deletions. (bottom) Example of a 7-bp deletion flanked by 3-bp microhomologies; the arrows in b and d indicate its genomic position and the sample in which it was found.

e, (top) Of all sequencing reads with an insertion, percentage which had a continuous match ≥ 6 bp between the "newly synthesised sequence" and the neighbouring sequences. Insertions generated during DSB repair in zebrafish are often accompanied with a multi-bp substitution (see Fig. 1h), they together form the "newly synthesised sequence" which is compared to the neighbouring sequences to find a possible match. Each bar represents an individual prime-edited larva. Darker green colours represent longer matches between the newly synthesised sequence and the neighbouring sequences, grey represents newly synthesised sequences with a < 6 bp match; that is, whose length was too short to analyse, or were untemplated, or used a template that was further away. There were 54–1535 reads with an insertion per larva. n = 41 samples. The "simulated" sample represents 1000 newly synthesised sequences generated at random. (bottom) Example of a 31-bp insertion with at least 19 bp templated from a neighbouring sequence (green); the arrows in b and e indicate its genomic position and the sample in which it was found.

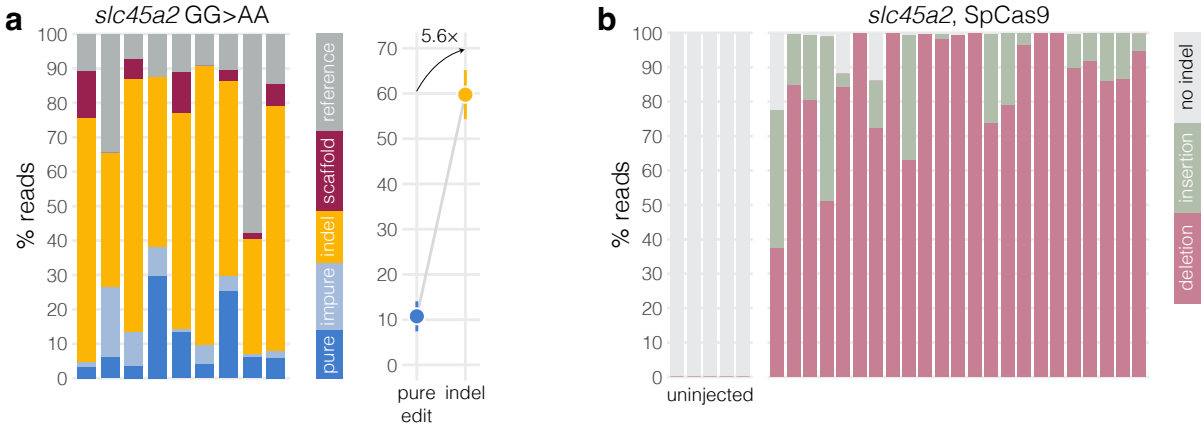

Supplementary Figure 8

Supplementary Fig. 8 | Prime editing and SpCas9 indels at *slc45a2* in wild-type embryos.
a, (left) Sequencing results from wild-type larvae injected with 30 fmol PEmax complexed with the *slc45a2* GG>AA pegRNA. Each bar represents an individual larva, with colours representing the percentage of reads assigned to each label. Minimum sequencing depth was 118×. n = 9 samples. The same samples are plotted in Supplementary Fig. 13. (right) The pure edit rate compared to the indel rate (mean ± SEM).
b, Sequencing results from wild-type larvae injected with 30 fmol SpCas9 complexed with gRNA targeting the same *slc45a2* locus (same spacer sequence) as in a. Each bar represents an individual larva, with colours representing the percentage of reads with an insertion, a deletion, or neither. Per larva, 98 ± 6% of reads carried an indel. Minimum sequencing depth was 788×. n = 23 injected samples.

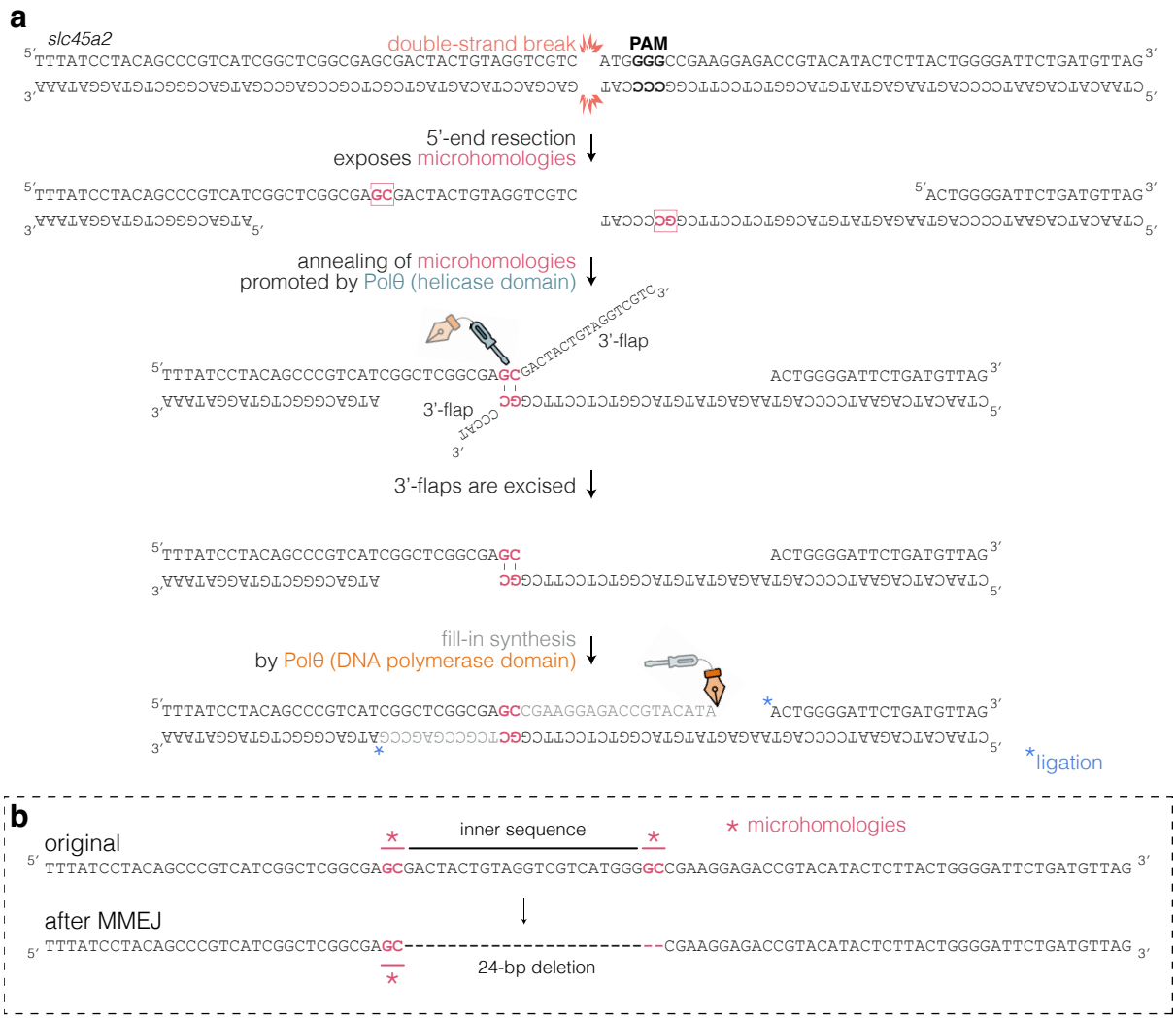

Supplementary Figure 9

Supplementary Fig. 9 | Canonical MMEJ mechanism generating microhomology-flanked deletions.

a, As example, simplified MMEJ mechanism creating a 24-bp deletion observed in embryos mutated with SpCas9 at the *slc45a2* locus (0.44—58% in 3/23 samples).

b, Mutation generated by the MMEJ mechanism in a. The typical MMEJ deletion removes the inner sequence between the two microhomologies and one microhomology. Whether the left or right microhomology is shown as deleted may be an arbitrary decision by the alignment algorithm.

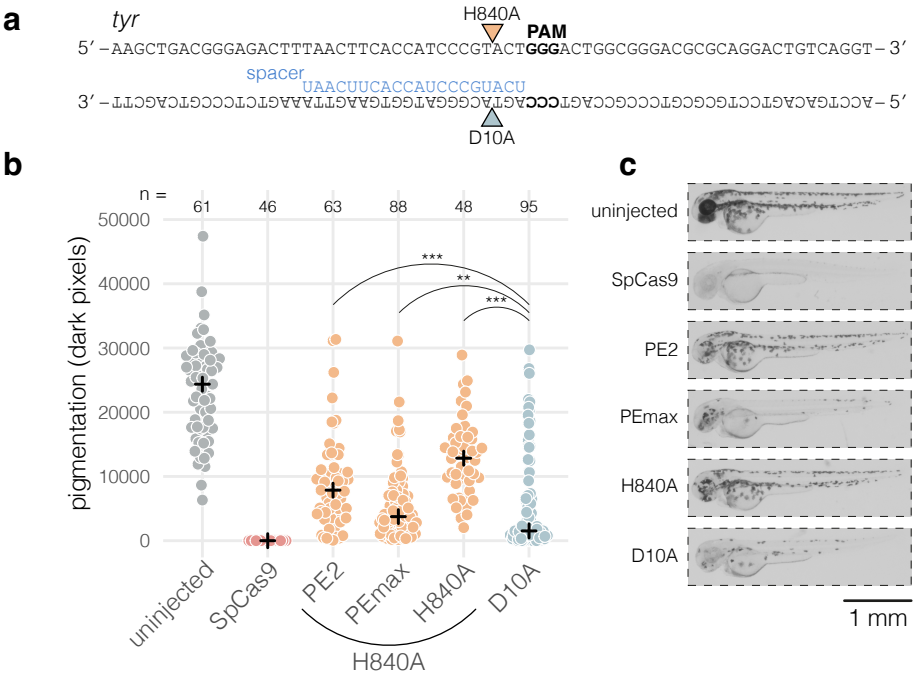

Supplementary Figure 10

Supplementary Fig. 10 | Cas9 nickases are highly mutagenic in zebrafish embryos.

a, At the *tyr* locus tested, the H840A nickases, which include PE2 and PEmax, cleave the 5′–3′ forward genomic strand; the D10A nickase cleaves the 3′–5′ reverse genomic strand; and Cas9 cleaves both strands.

b, Pigmentation of uninjected and injected larvae. Each dot represents the number of dark pixels per larva measured on pictures like in c. Black crosses mark the group medians. ** $p = 0.005$, *** $p < 0.001$ by Mann-Whitney U tests.

c, Example pictures of 2-dpf uninjected and injected larvae.

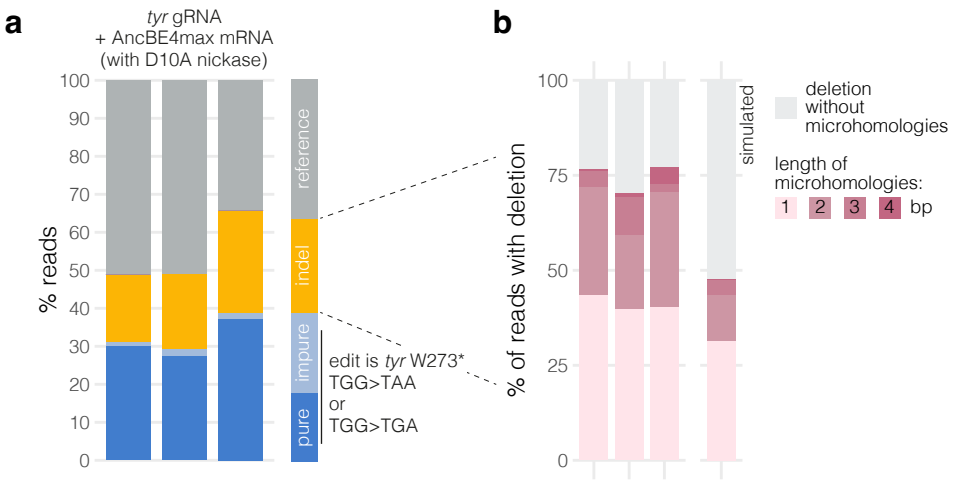

Supplementary Figure 11

Supplementary Fig. 11 | Base editing using the D10A nickase also generates deletions with signature of MMEJ.

a, Sequencing results from larvae injected with mRNA encoding the C-to-T base editor AncBE4max and a gRNA targeting *tyr*. Each bar represents sequencing data from a pool of zebrafish larvae, with colours representing the percentage of reads assigned to each label. Minimum sequencing depth was 44,859×. Sequencing data from Rosello et al., 2022 [11].

b, Of all sequencing reads with a deletion, percentage which show microhomologies flanking the deletion. Darker pink colours represent longer microhomologies, grey represents deletions without microhomologies. There were 7300–12,230 reads with a deletion per sample. The “simulated” sample represents 1000 deletions.

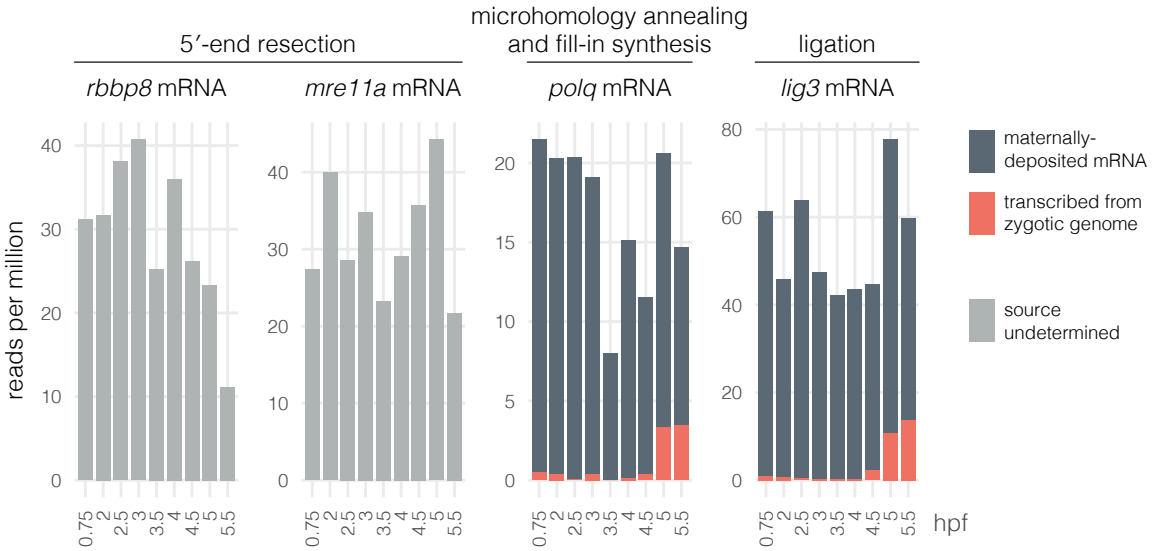

Supplementary Figure 12

Supplementary Fig. 12 | The main MMEJ factors are maternally deposited. Transcript levels of MMEJ factors during early zebrafish embryogenesis (0.75–5.5 hours post-fertilisation, hpf) in reads per million. Data is from Bhat et al., 2023 (Tables S4 and S5). As in virtually all metazoans, early zebrafish embryonic development relies on mRNA and proteins maternally deposited in the oocyte until the maternal-to-zygotic transition. The "SLAMseq" method distinguishes maternally-deposited mRNA from mRNA transcribed *de novo* from the zygotic genome by injecting single-cell zebrafish embryos with a uridine analogue which will only be incorporated in new transcripts. As can be seen from *polq* and *lig3* mRNA, the levels of zygotic transcripts only rise after the maternal-to-zygotic transition around 4.5–5 hpf, but levels of all four MMEJ factors presented here are high as early as 0.75 hpf, so are maternally deposited. Human *RBBP8* is often called *CTIP*, other genes have the same name as their human orthologues.

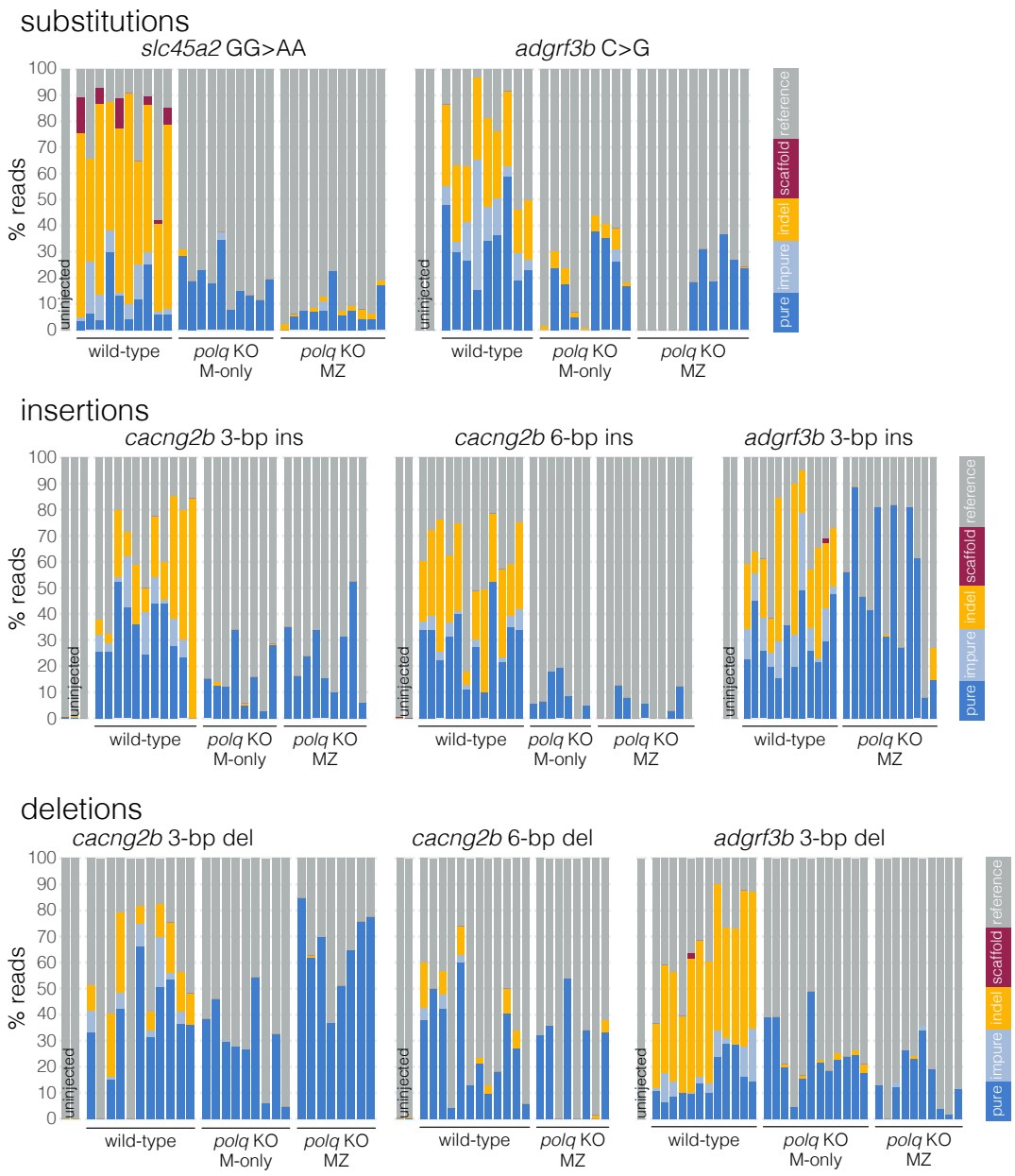

Supplementary Figure 13

Supplementary Fig. 13 | Prime editing in zebrafish embryos from homozygous *polq* KO mothers.

Sequencing results from wild-type, *polq* maternal-only heterozygous KO, and *polq* maternal-zygotic homozygous KO larvae uninjected or injected with PEmax complexed with one of 8 pegRNAs (9 edits in total with *cacng2b* G>C in Fig. 2d). Each bar represents an individual larva, with colours representing the percentage of reads assigned to each label. Minimum sequencing depth was 60×. n = 224 injected samples are plotted. *slc45a2* GG>AA wild-type samples are also plotted in Supplementary Fig. 8a. KO, knockout; M-only, maternal-only; MZ, maternal-zygotic.

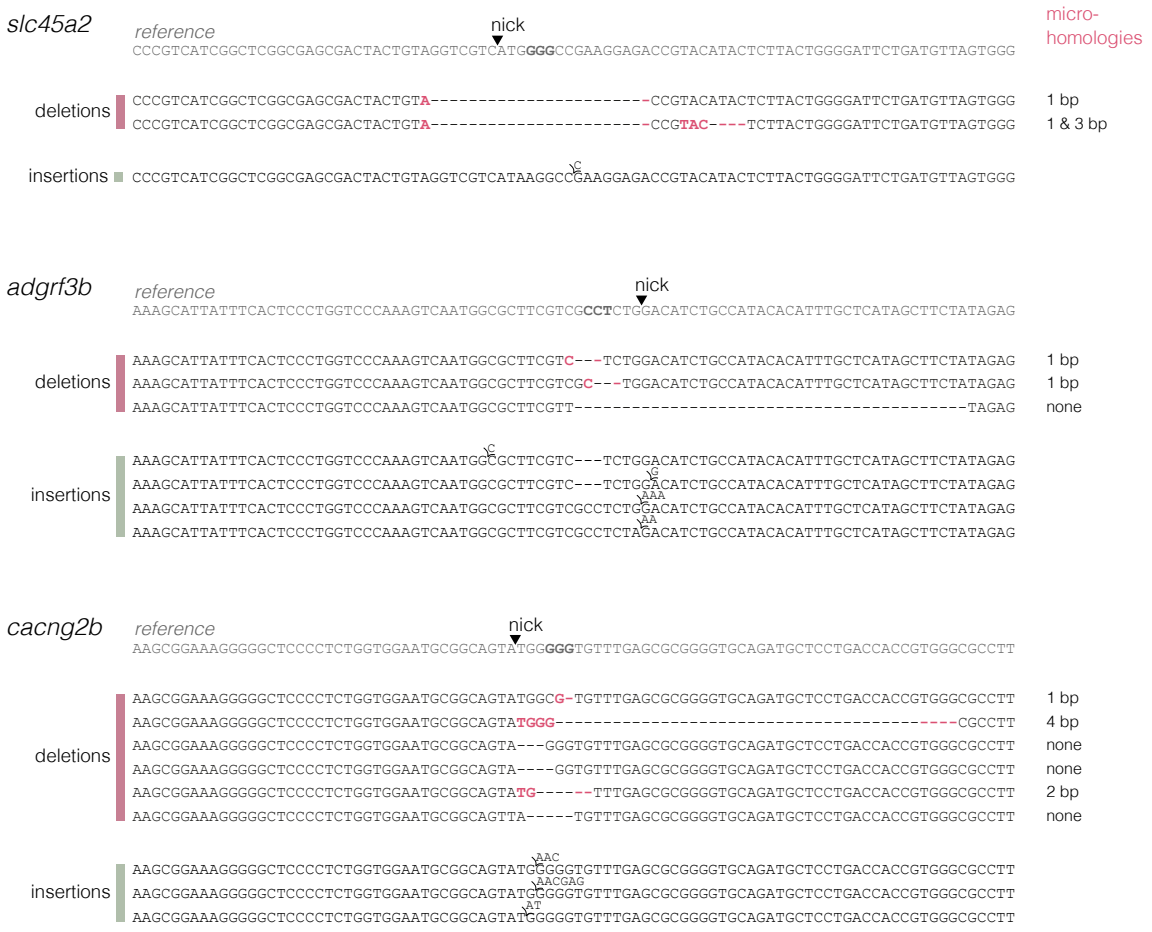

Supplementary Figure 14

Supplementary Fig. 14 | Remaining prime-editing indels in maternal-zygotic *polq* mutants.

Every indel observed after prime editing in *polq* maternal-zygotic homozygous KO. For deletions, microhomologies are written in pink and right column gives their lengths. The PAM is written in bold in the reference sequences.

Supplementary Figure 15

Supplementary Fig. 15 | Examples of insertions at the end of the RTT-templated nucleotides.

Every insertion at the *slc45a2* locus that is longer than 9 bp and starts exactly at the end of the RTT-templated nucleotides (nick + 16 bp). At the top is every unique insertion found in *slc45a2* AA>GG samples, except those injected with PEmax SpRY. At the bottom is every insertion found in *slc45a2* GG>AA samples. Inserted nucleotides are purple or green. In purple are inserted nucleotides likely templated from the scaffold because the inserted sequence starts with GGAC[...], which differentiates with GGAG[...] that could be templated from the end of the RTT-templated nucleotides.

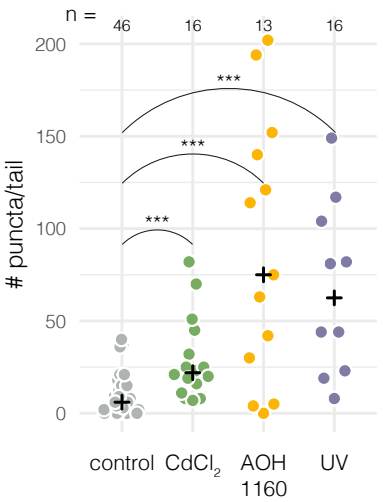

Supplementary Figure 16

Supplementary Fig. 16 | Acridine orange staining detects a rise in apoptotic cells caused by DNA damage.

Detection of apoptotic cells using acridine orange staining. Each datapoint represents the number of acridine-positive puncta in the tail of an individual 1-dpf wild-type embryo, either left untreated or treated directly after fertilisation with 20 µM CdCl2, or 20 µM AOH1160 for 24 hr, or UV radiation (~300 nm) for 30 min. Embryos were stained and imaged the next day at 1 dpf. Black crosses mark the group medians. *** $p < 0.001$ by Mann-Whitney U tests.

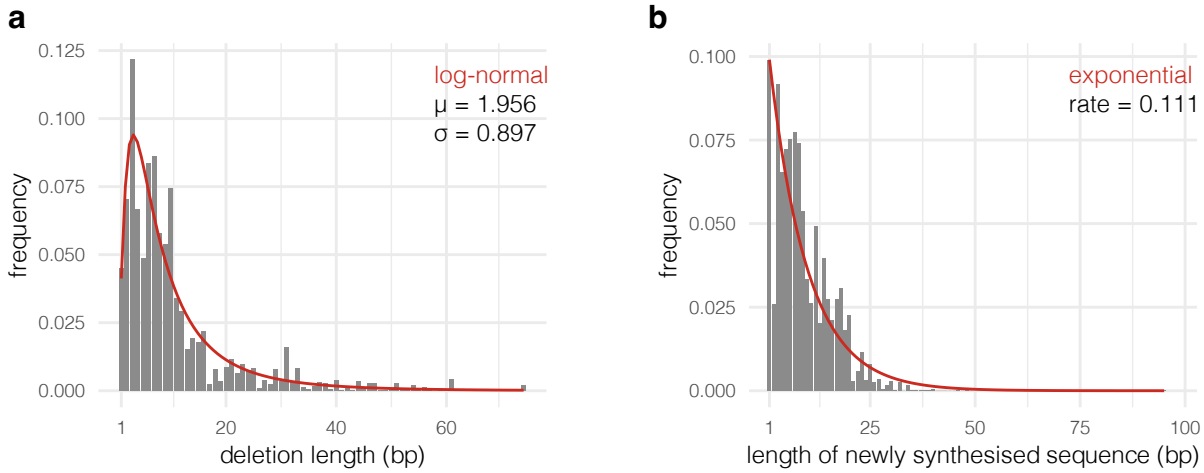

Supplementary Figure 17

Supplementary Fig. 17 | Distribution of deletion and insertion lengths after repair of Cas9 DSBs.

a, Deletion length frequencies observed in a dataset of n = 191 SpCas9-injected larvae mutated at n = 38 loci. The red curve is the fitted log-normal distribution. μ, location parameter; σ, shape parameter.

b, In zebrafish embryos, insertions generated during repair of a DSB often appear concomitantly with a multi-bp substitution (see example in Fig. 1k). We defined the "newly synthesised sequence" as the insertion together with the substitution if present. Here, frequencies of newly synthesised sequence lengths observed in a dataset of n = 191 SpCas9-injected larvae mutated at n = 38 loci. The red curve is the fitted exponential.